Journal of Environmental Chemical Engineering 10 (2022) 107322

Contents lists available at ScienceDirect

Journal of Environmental Chemical Engineering

journal homepage: www.elsevier.com/locate/jece

Agricultural and industrial waste-derived mesoporous silica nanoparticles: A review on chemical synthesis route

Nurina Adriana Abdul Razak [a], Nur Hidayati Othman [a,*], Muhammad Shafiq Mat Shayuti [a], Aidah Jumahat [b], Napisah Sapiai [b], Woei Jye Lau [c]

[a] Department of Oil and Gas Engineering, School of Chemical Engineering, College of Engineering, Universiti Teknologi MARA, 40450 Shah Alam, Selangor, Malaysia
[b] School of Mechanical Engineering, College of Engineering, Universiti Teknologi MARA, 40450 Shah Alam, Selangor, Malaysia
[c] Advanced Membrane Technology Research Centre (AMTEC), School of Chemical and Energy Engineering, Universiti Teknologi Malaysia, 81310 Skudai, Johor, Malaysia

ARTICLE INFO

Editor: Yang Liu

Keywords:
Agricultural waste
Industrial waste
Waste re-utilisation
Mesoporous silica nanoparticles
Pre-treatment
Chemical synthesis

ABSTRACT

In recent years, the amount of agricultural and industrial wastes being generated is increasing rapidly. This leads to numerous disposals, governance, and environmental issues. Therefore, the re-utilisation of these wastes into value-added products such as mesoporous silica nanoparticles (MSNs) has attracted great attention. MSNs have garnered immense attention in various applications owing to their tuneable pore dimensions, high surface areas, and tailorable structure, suitable for different post-functionalisation. In this review, recent progress on the synthesis of MSNs from waste using a chemical synthesis route is presented. This route offers the possibility to control silica structure, phase, morphology, and sizes by fine tuning the reaction parameters/conditions. The characteristics and applications of the MSNs produced are also analysed to examine the potential of using agricultural and industrial waste as the silica precursor. Although the use of inexpensive waste-derived materials seems promising for both waste reduction and value-added products synthesis, further research is still needed to boost the production of silica especially at a larger scale.

1. Introduction

Silica or silicon dioxide (SiO_2) has many remarkable properties such as controllable pore size, modifiable surface, strong mechanical properties, and a comparatively inert chemical composition, making it suitable for various applications [1]. It has been widely used in food and medical industries due to its safe and non-toxic nature [2]. Silica is also applied as additive in commercial epoxy resin and coating material because of its hydrophobicity properties [3]. Mesoporous silica nanoparticles (MSNs) refer to SiO_2 nanoparticles that have mesopores [4]. Many types of MSNs such as MCM-41 and SBA-15 with a wide range of pore geometries and particle morphologies have been synthesised. They exhibit high specific surface area, large pore size, chemical inertness, and a vast repertory of surface functional groups [5]. These unique features allow MSNs to be flexibly tuned for various applications such as adsorbents, catalyst supports, sensors materials, polymer reinforcement and other advanced composites [6–8].

Although silica can be found in almost every mineral on the earth, the synthesis of MSNs using a conventional method requires high temperature, which makes the process energy and cost consuming. The conventional method starts with the extraction of silica from silica source such as quartz sand to produce chemical precursors. These precursors are then used for the production of SiO_2. This conventional method contributes to global warming due to large amount of carbon dioxide (CO_2) emitted from the extraction process [9]. Stöber method is the most common method used to synthesise SiO_2 where sodium carbonate (Na_2CO_3) powder is heated with quartz sand at around 1300 °C to form silicate sodium (Na_2SiO_3) powder before reacting it with sulfuric acid (H_2SO_4). Typically, 0.53 tonnes of sodium carbonate (Na_2CO_3) and 0.51 tonnes of H_2SO_4 are used to produce 1 tonne of SiO_2. This leads to the production of 0.23 tonnes of carbon dioxide, 0.74 tonnes of sodium sulphate (Na_2SO_4), and 20 tonnes of effluents, all of which contribute to environmental issues [10]. Therefore, a more environmentally friendly and cost-effective approach is needed to synthesise SiO_2 nanoparticles.

Reutilisation of agricultural and industrial waste is an important strategy for long-term manner to achieve sustainable cycles in the industry [11]. The synthesis of nanomaterial from waste is considered an effective way to treat and recycle waste. This adheres to the concepts of

* Corresponding author.
E-mail address: nurhidayati0955@uitm.edu.my (N.H. Othman).

https://doi.org/10.1016/j.jece.2022.107322
Received 1 October 2021; Received in revised form 10 January 2022; Accepted 1 February 2022
Available online 3 February 2022

minimum waste generation and waste-to-wealth mission. Some of the possible industrial wastes that can be reutilised for SiO_2 synthesis include powerplant fly ash [12], rice husk ash [6,13], sugarcane bagasse ash [14], and palm kernel shell ash [11,15]. The agricultural and industrial wastes, particularly their ashes, are considered as potential raw material for the production of SiO_2 due to the continuous ash generation and its high silica content.

Fly ash (FA) is a by-product of thermal power plant combustions containing both amorphous components such as SiO_2, Al_2O_3, Fe_2O_3, Fe_3O_4, TiO_2, CaO, and crystalline phases such as quartz and mullite [16]. It has been used as a filler and construction material [17]. Besides, numerous studies have focused on FA as an aluminosilicates source due to its high silica content [18]. In addition to the FA, the use of agricultural wastes such as rice husk, sugarcane bagasse, and coconut shells for the synthesis of nanomaterials particularly silica has been progressively carried out as these wastes are low-cost renewable resource and contain relatively high silica content. This review highlights the re-utilisation of waste particularly agricultural and industrial for the production of silica using the chemical routes. This review also emphasises the importance of chemical treatment parameters towards the final properties of the synthesised MSNs. In addition, the characteristics and applications of the MSNs are also discussed.

2. Routes to synthesis mesoporous silica nanoparticles (MSNs)

Several techniques have been developed to synthesise and produce MSNs with controlled shape, size, dimension, and structure from different waste materials such as rice husk ash, coal fly ash, paddy husk ash, and others. The techniques for extracting silica particles can be classified into two [19], which are top-down or physical approach and bottom-up or chemical approach as illustrated in Fig. 1. The top-down approach is defined by applying special size reduction techniques to reduce the dimension of the original size. Meanwhile, the popular method for producing MSNs from the atomic or molecular scale is the bottom-up approach [20]. Lithography [21] and milling [22] are some examples of silica nanoparticles synthesis using the top-down approach. Chemical vapour deposition (CVD), hydrothermal synthesis, microemulsion technique [19], sonochemical technique [23], co-precipitation [24], and sol-gel technique [25] are the examples of silica nanoparticles synthesis using the bottom-up approach.

2.1. Top-down approach

Top-down or physical approach is defined by reducing the dimension of the original size by using special size reduction techniques [26]. This approach is generally more straightforward and relies either on bulk material removal or division or on miniaturisation of the bulk fabrication processes to achieve the desired structure/surface properties [27]. The milling technique is an example of a top-down approach that breaks down bulk materials to reach fine particles [28]. Ball milling is a shear-force dominating technique in which the particle size is reduced by impact and attrition. It uses metallic balls (usually Zirconia or steel balls) as a grinding media and a rotating shell to produce centrifugal force [29].

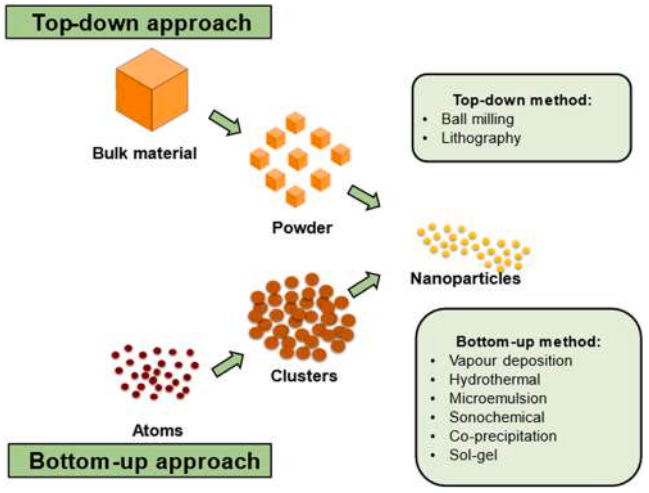

Fig. 1. Top-down and bottom-up approaches.

This technique offers a number of benefits including cost-effectiveness, high product purity, low-temperature reaction, controllability, facility, and reproducibility [30]. Meanwhile, nanolithography is a technique for creating nanoscale structures that involves pressing a mould with three-dimension (3D) surface patterns against a superheated cast [31]. To achieve high-resolution topography, lithography is generally coupled with deposition and etching. Masked lithography and maskless lithography are the two types of lithography. Masked lithography includes photolithography [32]. Photolithography, the semiconductor industry's reliable technique for high-volume production, has been used directly to produce discrete monodisperse colloidal particles. This technique offers several distinct benefits including exceptional shape consistency up to the submicrometer level and excellent output [33].

However, top-down synthesis method needs further improvement due to the formation of flaws in the structure of the produced material. This is a significant limitation since the surface chemistry and other physical characteristics of the nanoparticles are strongly dependent on the material structure. In addition, they might have a lot of contaminants in the produced material. Despite these main drawbacks, this method is considered suited for large-scale manufacturing as it allows for deposition over a large substrate and requires no chemical purification [34].

2.2. Bottom-up approach

The bottom-up approach includes a chemical aggregation of MSNs from atom to atom or molecule to molecule [19]. This technique is considerably more prevalent for nanoparticle elaboration because it allows for precise particle size control. Bottom-up approaches are more versatile in which this method has resulted in a wide range of nanoparticle synthesis methods based on the self-assembly principle [34]. The significant advantage of this method is the high yield purity [35].

CVD is a process where vapour-phase substances are condensed to form a solid-phase material [36]. It is a well-known chemical technique utilised in a variety of industries for high-temperature protection, erosion protection, and a combination of the two [37]. According to Huang et al. [38], CVD is the most common method to produce large-scale and high-purity fumed silica glass. This process involves injecting a precursor into H_2/O_2 flame to synthesise SiO_2. The silica glass is then formed by transporting SiO_2 to the substrate and depositing it on the substrate; hence, SiO_2 production inside a chamber is crucial to control this process. In an industry, halide compounds such as silicon tetrachloride ($SiCl_4$) are widely utilised as a precursor for CVD synthesis of silica glass. However, this technique requires high temperatures and its growth rate is rather slower. Furthermore, it utilises hazardous reagents such as $SiCl_4$, $Ni(CO)_4$ and B_2H_6. Some of these reagents are highly explosive and corrosive [39].

In addition to CVD, hydrothermal synthesis is another method to produce silica. In general, hydrothermal processes are carried out in a high-pressure enclosed compartment under subcritical or supercritical solvent conditions [40]. The utilisation of traditional hydrothermal method exhibits some drawbacks including poor yield, extensive process durations, and heterogeneous structure. This flaw may be remedied by utilising a microwave as a heater [41]. This method allows the control of the resulting nanoparticles morphology [42], able to produce material that is unstable near the melting point, and large crystals of high quality

[34]. However, it requires high temperature furnace and heating devices [39]. Fernandes et al. [43] synthesised MSN KIT-6 via hydrothermal synthesis whereby hydrochloric acid (HCl) was used to keep the medium acidic, the triblock copolymer *P123* as an organic structural template, and tetraethylorthosilicate (TEOS) as a source of silica. Silmi et al. [40] reported that hydrothermal is one of the most well-known and successful synthesis techniques for generating MSN KCC-1 with tuneable pore and particle size.

Furthermore, microemulsions are self-aggregated colloidal system that gives a controllable system with potential use of nanoreactors. They can function as pools within which nanoparticle characteristics may be easily regulated [44]. According to Narayan et al. [4], this approach is presented as a new MSNs synthesis technique. This method is able to control the size, shape, and crystal structure of the metallic nanoparticles; thus, generating a series of seeds with various shapes and sizes using the same reagents. Furthermore, controlling reaction duration, temperature, and reaction conditions will create various geometries that could be potentially used in many research fields [44]. However, this method requires a large amount of surfactant and its stability is influenced by the pH of the microemulsion [34].

Sonochemical synthesis was one of the first techniques developed to produce engineered nanomaterials [45]. Ultrasound irradiation is a simple way to make a range of nanomaterials from inorganic precursors, mostly by primary, secondary or combined sonochemistry effects. When the secondary sonochemical synthesis uses the post-produced chemical consequences in the liquid phase, the primary sonochemical synthesis refers to the extreme transitory circumstances such as high pressure and temperature from the collapse of the cavitation bubbles [46]. Thus, this high-intensity ultrasound offers a unique approach to nanoparticle synthesis that avoids the need for bulk high temperatures, high pressures or extended reaction periods [42]. However, this method produces low materials yield [34].

Chemical precipitation is a prevalent method in synthesising silica nanoparticles due to its energy efficiency and excellent processing time [24]. Another effective soft chemical route to mix oxide materials is the co-precipitation technique or known as the solid-state analogue or a side-branch of the sol–gel process [47]. Co-precipitation reactions occur when nucleation, growth, coarsening, and/or agglomeration processes happen at the same time. This technique is simple, allows easy size and deposition control, requires minimal temperature, and is energy efficient [48]. It also has the benefit of producing homogenous nanomaterials with small size and size dispersion directly into the solution through various chemical reactions [49]. However, Rane et al. [48] stated that this approach is not applicable to uncharged species and the product obtained may include precipitated trace impurities. Furthermore, it suffers from batch-to-batch reproducibility issues.

Lastly, because of its ability to produce a pure and homogenous product under mild circumstances, the sol-gel method has been frequently utilised to produce MSNs [19]. It is a simple, economical, and efficient method in producing high quality coating [34]. However, this synthesis technique necessitates the use of expensive raw materials and a high-temperature furnace or heating apparatus [39]. In the presence of acid or base, this process includes the hydrolysis and condensation of metal alkoxides such as TEOS ($Si(OEt)_4$) or inorganic salts such as Na_2SiO_3 [4,19]. The dimensions and morphologies of the resultant materials are influenced by temperature, water content, pH, surfactant or copolymer properties, and the concentrations and sources of the silica employed in the process [5].

2.3. Comparative assessment of silica production methods

Majority of commercial silica extraction methods are both costly and time consuming [9]. The Stöber method is used to synthesise monodispersed silica particles in the sub-micrometer range [50]. In this process, tertraethylothosilicate (TEOS)undergoes hydrolysis, followed by a polycondensation reaction to produce non-porous silica particles. Besides TEOS, a number of low cost silica precursors such as Na_2SiO_3 solution have been used [4,19]. Sometimes, surfactants are also added to control the pore size of MSNs. Appropriate control of pore sizes is very essential especially when the MSNs are used as a support material to load different components.

The synthesis of MSNs is much more expensive than conventional silica as it has higher specific surface area, pore volume and unique pore size. As a result, extracting MSNs from waste can be both cost-effective and environmentally friendly. Table 1 compares several aspects of silica production using various methods in terms of process, cost, practicality and safety aspects. When compared to industrially used methods, silica recovered from waste treated with alkali gives high purity silica at a low temperature. By dissolving waste in sodium hydroxide (NaOH) solution, Na_2SiO_3 could be easily obtained, and silica can be quickly precipitated from solution using sol-gel process [9]. A few ways for obtaining silica from waste and other commercial sources have been reported. In comparison to conventional method, physical method is an easy straightforward, cost-effective and environmentally friendly method. However, the silica produced by this method have flaws in their structure and they tend to be contaminated during the process. In terms of practicality, this method is reproducible and suited for a large scale-manufacturing. Besides, chemical method is one of the most used methods in producing MSNs due to its simplicity and ease of process. Although this method is able to produce high purity MSNs, this method is not practical due to its expensive cost, non-environmentally friendly and high temperature requirement. The raw materials used such as TEOS, tetramethylorthosilicate (TMOS), methyltriethoxysilane (MTES) and polyethoxydisiloxane (PEDS) [51] are expensive and they are subjected to high temperature synthesis process. In terms of environmental aspect, this method uses inorganic acid which requires proper disposal due to its non-environmental friendly nature. On the other hand, green chemical method is considered simple although it requires pre-treatment step of the waste. It is also cost-effective due to the usage of inexpensive chemicals. In terms of practicality and safety, it can be produced at a larger scale and does not require high temperature equipment.

3. Chemical treatment for silica production

Many works have investigated the use of industrial waste particularly FA to produce SiO_2 nanoparticles. Most of the approaches are based on the chemical route due to the simplicity of the process. Fig. 2 shows the general procedure for the chemical treatment process in producing SiO_2 nanoparticles. In general, there are three main processes under chemical treatments, which are acid leaching treatment, alkaline treatment, and silica recovery. Acid leaching is an effective pre-treatment process to remove organic matter and metallic impurities in the waste [52]. By incorporating the acid leaching treatment method, the yield and purity of the silica increase significantly [52] and a higher surface area of a silica product could be obtained [53]. This is because acid leaching treatment affects the chemical composition of the waste [53]. According to Kwan and Wong [52], acid-treated waste exhibits a low degree of silica crystallisation during combustion process. The crystallisation catalyst has been removed, and the waste becomes less sensitive to the combustion temperature. The combustion process under controlled temperature produces acid-treated waste that contains rich amorphous SiO_2, low alkali oxides, low unburnt carbon, smaller particle size, and large specific surface area compared to the non-acid treated waste.

After the acid leaching treatment process, the pre-treated waste undergoes alkaline treatment to form a Na_2SiO_3 solution. Alkaline treatment is an essential step in disrupting the waste's compact structure and enhancing the silica yield. This is because the bonds between silica and other components in the waste are broken down and dissolved into an alkaline medium called Na_2SiO_3 solution [54]. According to Anuar et al. [55], silica does not react with water due to its weak acidic nature. Silica only reacts with strong bases reagents such as KOH and NaOH. As

Table 1
Comparison of silica production method.

Method	Ease of process	Economics	Environmental	Practicality	Safety	Final silica properties produced
Chemical method (sol-gel)	Simple [34]	Requires expensive raw materials and high temperature furnace [39]	Not environmentally friendly due to the usage of inorganic acid [4,19]	Not practical for industrial scale	Requires high temperature [39]	High purity MSNs can be produced
Green chemical method	Simple but requires pre-treatment step	Cost-effective due to the usage of inexpensive chemicals	Environmentally friendly due to the usage of organic acids	Reproducible in a large-scale manufacturing	Doesn't require high temperature	The purity depends on pre-treatment and synthesis conditions
Physical method	Easy and straightforward [27]	Cost effective [30]	Environmentally friendly [34]	Reproducible in a large scale manufacturing [34]	Requires low temperature [30]	Difficult to obtain high purity and nanosized silica
Commercial method	Complicated and time-consuming [9]	Expensive. Requires expensive pre-cursors and high-temperature equipment [9]	Large amount of CO_2 emission during extraction process [9]	Longer time and higher temperature process	Requires high temperature of up to 1300 °C [9]	High purity MSNs can be produced

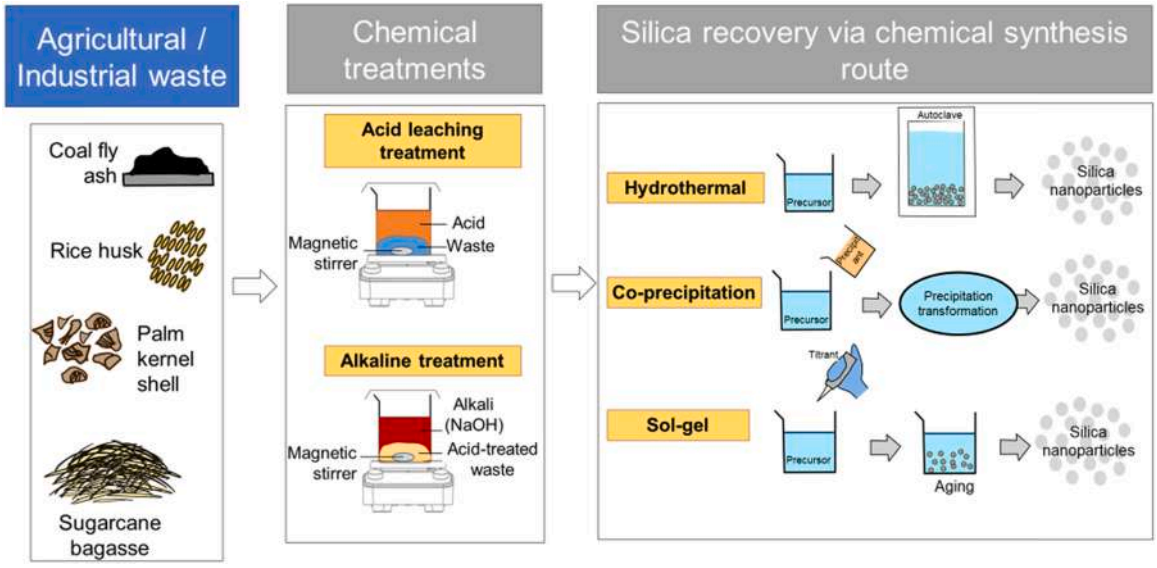

Fig. 2. Simple procedure of chemical treatment process for silica production.

a result, the only way to extract silica from waste is to dissolve it in a strong alkaline solution.

The final stage of the process is the recovery of the silica through the precipitation route. Under the recovery stage, several available methods can be used such as hydrothermal synthesis [19], co-precipitation technique [24], and sol-gel process [25]. In the precipitation route, precipitants typically acid solutions are added into the alkaline silicate solution to promote the formation of silica due to the Na^+ exchange from the alkaline silicate structure to the acidic solution [55]. The pH of the alkaline silicate solution needs to be adjusted in order to obtain silica particles [56]. This is because silica solubility increases as the pH of a solution rises. Thus, the basic requirement is to use acidic reagents to lower the pH of the alkaline silicate solution.

3.1. Acid leaching treatment

Chemical leaching is a process to extract metal from a solid phase to a liquid solution using acids or bases, surfactants, chelating agents, salts or redox agents [57]. This is because chemical leaching is an effective pre-treatment process to remove or reduce the concentration of toxic metals in the waste to obtain a higher yield and purity of desired products such as silica [52]. The chemical leaching process is also used to recover metal waste, which may be considered as a source of valuable metals that would otherwise be disposed of in landfills; hence, causing environmental issues [58]. Typically, acidic solutions are used to recover metals by using suitable leachates, which cause the dissolution of the metallic fractions of the waste. Finally, the metals from the waste are leached out into the solution [59]. The ash reaction with an acid solution such as HCl can be expressed as follows [60]:

$$3Al_2O_3 \cdot 2Si_{2(s)} + 18HCl_{(l)} \rightarrow 6AlCl_{3(aq)} + 2SiO_{2(s)} + 9H_2O_{(l)} \quad (1)$$

Several acids can be used for acid leaching treatment such as HCl [14], sulfuric acid (H_2SO_4) [52,61], citric acid ($C_6H_8O_7$), acetic acid (CH_3COOH), oxalic acid ($C_2H_2O_4$) [62], and nitric acid (HNO_3) [52,63]. The selection of acid generally depends on the metal content in the waste, and the presence of inert elements or poisonous compounds [64]. Azat et al. [53] found that treating rice husk ash with HCl could remove trace elements such as K_2O, CaO, MnO, and ZnO from the waste and improve the purity of the final silica produced.

Gao et al. [62] compared the performances of four acidic solutions HCl, CH_3COOH, $C_2H_2O_4$, and $C_6H_8O_7$ towards product distribution (Fig. 3 (a)). It was observed that after the leaching treatment, trace elements such as Na_2O, Al_2O_3, and Fe_2O_3 could still remain in the silica product but at a very low concentration due to the phase transformation from oxides to soluble ions (Fig. 3**(a)**). Higher SiO_2 purity was obtained from all three organic acids compared to the inorganic acid, suggesting organic acids have a more significant leaching effect. Xu et al. [65] stated that an acid leaching treatment on rice husk waste affects the

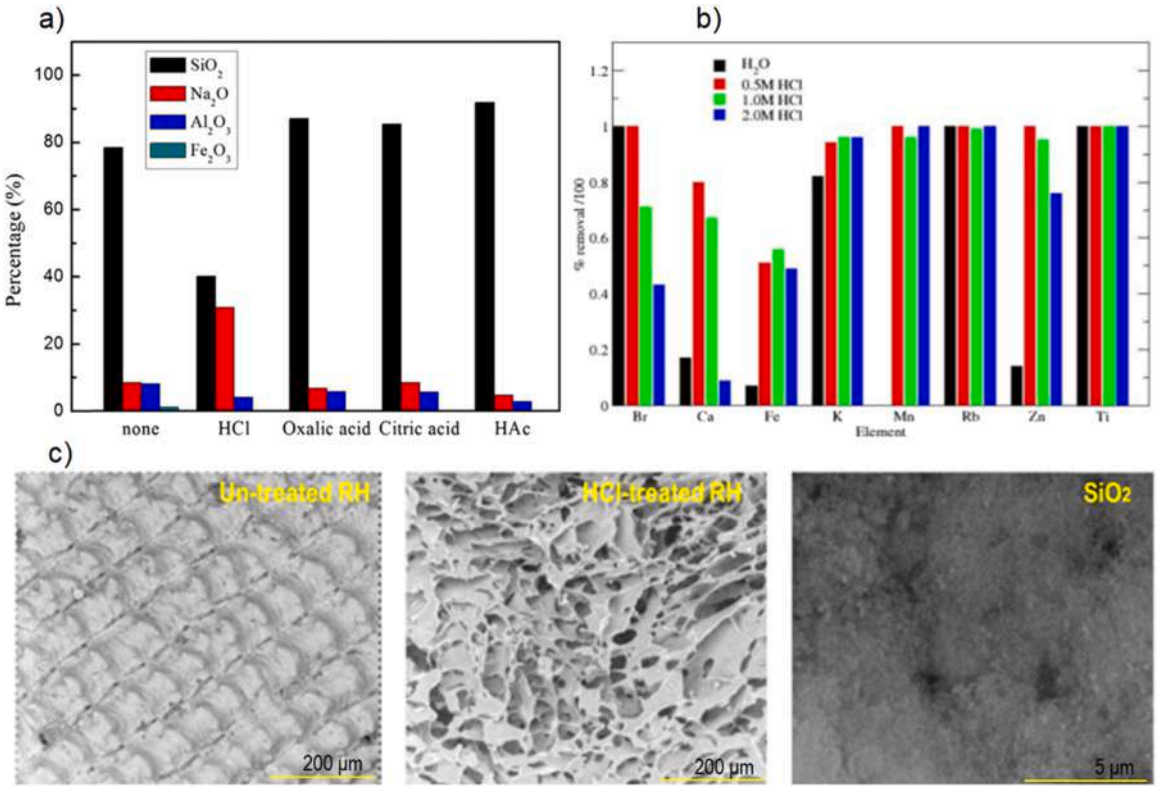

Fig. 3. Effects of a) acid types on product distribution [62]. HCl concentration on the percentage removal of impurities based on XRF analysis [68]. SEM images risk husk (RH) and SiO_2 [53].
(a) Reprinted with permission from Elsevier. (b) Reproduced from IOP Publishing and c) Reproduced from TÜBİTAK academic journals.

trace element content in the waste. HCl was found to be more effective in eliminating metallic impurities compared to other leaching agents. The trace amounts of K_2O, Na_2O, CaO, MgO, Al_2O_3, and Fe_2O_3, were reduced to relatively low levels, particularly potassium. HNO_3 and H_2SO_4 performed well in removing alkali metals, increasing the surface areas and lowering the carbon residue percentage of the waste.

Farirai et al. [14] treated sugarcane bagasse ash with $C_6H_8O_7$ in which metal impurities such as Al_2O_3, Fe_2O_3, MnO, and CaO were significantly reduced after the leaching treatment, yielding to 98.92% amorphous silica. Nassar et al. [6] investigated the use of HNO_3 followed by H_2SO_4 for the acid leaching treatment of rice husk (RH). It was found that the acid addition sequence for acid leaching and titration steps play a vital role in determining the purity, yield, and crystallite size of the synthesised silica product. The combination of both acids removed Ca ($Al_2SiO_2O_8$), resulting in a single-phase product of silica that is cristobalite beta. Azat et al. [66] found that even though HCl pre-treatment could lead to greater purity products, $C_6H_8O_7$ pre-treatment might be considered as an alternative solvent due to its lower cost and environmental impact. In order to enhance the leaching pre-treatment efficiencies to eliminate organic and metallic impurities, the solution's concentration, reaction time, and temperature should be controlled appropriately [56].

The recovery of metal can be significantly affected by acid concentration due to the H^+ concentration [67]. Librea et al. [68] compared the performance of different HCl concentrations (0.5 M, 1 M, and 2 M) for RH. After being leached with 2 M HCl, the impurities of Mg, Al, K, Ca, Rb, Ti, and Mn were undetectable. Cl, on the other hand, was found in the acid-treated waste as a result of trapped acid in the rice husk fibres. Due to the elimination of impurities, Si content was observed to rise due to the leaching treatment (Fig. 3 **(b)**). With 0.5 M HCl, the removal of Ca, Fe, K, Mn, and Zn was more effective. When compared to these metals' ionic forms, H^+ was more reactive. H^+ can displace these ions in the waste matrix; thus, allowing for efficient metal impurity leaching. However, it was discovered that when the acid leaching concentration increased, the leaching efficiency declined accordingly. Therefore, it was concluded that 0.5 M HCl is the best concentration to be utilised for acid leaching of waste for silica synthesis.

It is worth noting that acid leaching treatment can significantly increase the waste's surface area, pore volume, and pore diameter. This is because, following the leaching treatment, the hydrolysis of lignin and cellulose into smaller compounds and the dissolution of alkali metals promote the volatilization of fixed carbon in the waste. Furthermore, eliminating organic carbohydrates cause the waste's internal pores to open, resulting in a looser and porous waste structure formed. Fig. 3 **(c)** shows the scanning electron microscopy (SEM) images of the RH with and without HCl pre-treatment. A significant structure breakdown was observed for the HCl-pre-treated RH due to acid delignification and therefore, amorphous SiO_2 with 50 nm could be obtained [53]. There was a difference of less than 3% in the total weight loss between acid-treated and untreated waste, indicating that the leaching treatment impacted the waste's thermal stability. However, it must be pointed out that inorganic acid is not environmentally favourable due to the need for expensive corrosive resistant processing equipment and specific disposal treatment of the used acid [61].

Chindaprasirt and Rattanasak [69] pre-treated bagasse FA with a lower HCl concentration (1 M HCl) and discovered that the quantities of metal oxides (Al_2O_3, CaO, SO_3, MgO, and K_2O) were reduced due to the interaction with the acid, particularly CaO. The metal elements, on the other hand, interacted with HCl producing a chloride salt solution. Furthermore, since the acidic solution did not react with carbon, the LOI of the treated waste showed no changes. However, it was also determined that the acid leaching treatment had no substantial impact on the waste's morphology. Meanwhile, Steven et al. [70] compared the performance of three different acid leaching sequences of rice husk waste for silica extraction. It was discovered that acid leaching performed before the additional treatments resulted in pulverised waste and

lowered the void fraction. As a result, reduced bulk volume on the sample was reported. Therefore, agitation was introduced to make the extraction process easier. The leaching process removed the majority of impurities and increased the silica purity.

Leaching efficiency is also affected by the operating temperature [71]. Zhao et al. [72] discovered that the removal effect of Al, Ca, and Fe at 85 °C was better from bauxite reaction residue compared to Ti. This is because Ti is primarily existed in the form of rutile and anatase, making it difficult to leach out at low temperature. The leaching procedure was also discovered to efficiently break down the structure of poly-aluminium chloride (PAC) and converted it to aluminium chloride solution. Due to the lack of PAC, it also eliminates Cl^-. As a result, prior to the leaching procedure, the removal rate of Al, Ca, Fe, and Ti also rises. Osman and Sapawe [73] conducted acid leaching treatment on oil palm frond waste at a slightly lower temperature of 70 °C. The findings showed that leaching treatment reduced the amount of inorganic oxide in the waste. This removal was based on the principle that the acid's carboxyl groups serve as a chelating agent by donating H^+ and forming stable complexes with metal ions. As a result, positively charged ions such as K^+, Ca^+, and Mg^+ were significantly reduced following leaching treatment, whereas Fe content was eliminated. Usgodaarachchi et al. [74] treated rice husk with HCl at 80 °C and discovered that metallic impurities including Fe^{3+}, Ca^{2+}, Na^+, K^+, and Mg^{2+} could be eliminated. The treated waste was white compared to the untreated waste, which was light brown. As a result, the purity and colour of the silica products were affected.

Lastly, leaching time also affects the leaching efficiency of a waste. According to Gao et al. [75], the leaching rate of Fe from coal FA gradually increased between zero and 2 h and started to reach a plateau after 2 h. It was concluded that the optimal leaching time was 3 h. Bain et al. [76] treated bottom ash with $C_6H_8O_7$ and HCl for 12, 20, 48, and 72 h to study the effect of time taken on heavy metal removal efficiency. When the bottom ash was immersed for 20–72 h, the efficiency of $C_6H_8O_7$ increased, and the removal efficiency of As improved. However, it was also noted that with $C_6H_8O_7$, the removal efficiency of Cu and Zn declined with time. HCl was able to remove metal impurities in 12 h leaching time due to its strong acid nature by dissolving metal ions that were released into the acidic solution.

Faris [77] also studied the effect of leaching time on removing impurities from mustard husk ash. After 25 min leaching, it was discovered that the amount of SiO_2 increased, Al_2O_3 was eliminated, and other impurities were reduced. Although, there was no optimal improvement in SiO_2 purity, Al_2O_3 and MgO were able to be removed together with other impurities were reduced after more than 50 min leaching. Fe_2S levels were also found to increase when the leaching was carried out for up to 90 min leaching. According to the findings, the optimal leaching time for mustard husk ash was 50 min Table 2 summarises some of the synthesis parameters used by previous studies for acid leaching treatment.

3.2. Alkaline treatment

Alkaline treatment is a process producing Na_2SiO_3 solution from raw materials using NaOH solution. The reaction of the obtained product from ash can be written as Eq. (2) [78]:

$$NaOH + SiO_2 \rightarrow \quad Na_2SiO_3 + \quad H_2O \tag{2}$$

There are many parameters such as concentration, temperature, and operating time that need to be controlled in alkaline treatment. These parameters affect the purity, crystallinity, and surface area of the silica product. According to Fajaroh et al. [79], the concentration of the alkaline solution affects the crystallinity and specific surface area of the particles. To produce the intermediate monomer structure, the simplest amorphous silica only has to separate two Si–O links based on the bond energy alone. Quartz, on the other hand, requires the breaking of four Si–O bonds and a single Si–O bond, which is generally produced using a high-pressure hydrothermal process (Fig. 4) [72]. Zhao et al. [72] also discovered that the alkaline treatment's reaction temperature affected the silica extraction rate. This is due to the amorphous silica's strong dissolving capabilities. Meanwhile, operational treatment time has an impact on the silica solubility, which influenced the silica's purity and crystallinity.

One parameter that significantly affects the silica product obtained from Na_2SiO_3 solution is the alkaline concentration. According to Fajaroh et al. [79], the higher the concentration of the silicate solution, the smaller the crystallinity of the particles generated and the bigger the

Table 2
Previous studies on extraction of silica using different acid leaching parameters.

Raw material	Investigation parameters				Impurities removed/reduced	Reference
	Type of acid	Concentration	Temperature (°C)	Duration (h)		
Rice husk ash	HCl, H_2SO_4, HNO_3	1 N, 3 N, 3 N	ambient	1, 2.5	Reduce impurities such as K_2O, Na_2O, CaO, MgO, Al_2O_3, and Fe_2O_3	[65]
Fly ash	HCl, CH_3COOH, $C_2H_2O_4$, $C_6H_8O_7$	–	25	1	Remove impurities such as Na_2O, Al_2O_3, and Fe_2O_3	[62]
Sugarcane bagasse ash	$C_6H_8O_7$	5% in 500 mL	90	3	Reduce impurities such as Al_2O_3, Fe_2O_3, MnO, and CaO	[14]
Rice husk ash	HNO_3, H_2SO_4	2 M	80	3	Remove $Ca(Al_2SiO_2O_8)$	[6]
Rice husk	HCl	2 M	–	–	Remove impurities such as K_2O, CaO, MnO, and ZnO	[53]
Rice husk	HCl	0.5 M, 1 M, 2 M	–	48	Remove impurities such as Mg, Al, K, Ca, Br, Mn, Rb, Zn, Ti, and Fe	[68]
Bagasse fly ash	HCl	1	25	2	Reduce impurities such as Al_2O_3, CaO, SO_3, MgO, and K_2O	[69]
Rice husk ash	HCl	1	100	1	Reduce most impurities	[70]
Rice husk	HCl, $C_6H_8O_7$	2	90	2	Reduce impurities	[66]
Bauxite reaction residue	HCl	8	85	3	Reduce impurities such as Al, Ca, Fe, and Ti	[72]
Oil palm frond ash	$C_6H_8O_7$	–	70	1	Reduce impurities such as K, Ca, and Mg Remove Fe completely	[73]
Rice husk	HCl	–	80	5	Remove impurities such as Fe, Ca, Na, K, and Mg	[74]
Coal fly ash	HCl, H_2SO_4, HNO_3	–	55, 65, 75, 85, 95	1, 2, 3, 4	Remove Fe	[75]
Powerplant bottom ash	$C_6H_8O_7$, HCl	–	70	12, 20, 48 72	Remove impurities such as Cu, Zn, and As	[76]
Mustard husk ash	$C_6H_8O_7$	1, 2, 3, 4, 5, 6	25, 60, 80, 95	0.4, 0.8, 1.5, 2, 3	Remove impurities such as Al_2O_3 and MgO Reduce impurities such as KCl, Fe_2S, and Ca	[77]

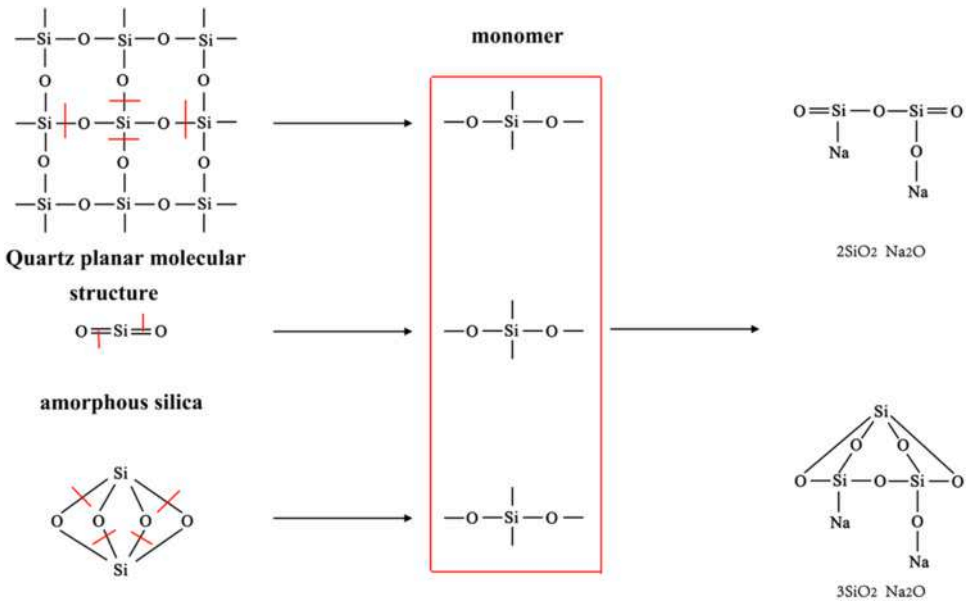

Fig. 4. The molecular structure of sodium silicate made from quartz and amorphous silica [72]. Reproduced from De Gruyter.

specific surface area of the particles produced. Farirai et al. [14] conducted an alkaline treatment process of sugarcane bagasse ash using 2 M NaOH solution. High purity amorphous silica of 98.92% in nanosize ranging from 6 to 24 nm and a high specific surface area of 240 m^2/g was successfully obtained. The alkaline treatment during the synthesis stage developed particle agglomeration that resulted in clusters. The surface area of the synthesised silica was also superior compared to the commercial silica utilised in the study.

Furthermore, Zhao et al. [72] compared the silica extraction rate of five different concentrations (1 M, 2 M, 3 M, 4 M, and 5 M) of NaOH solution used during the alkaline treatment. When the concentration of NaOH solution was increased from 0 to 5 M, the silica extraction rate increased from zero to 85.66%. The concentration of NaOH had a considerable impact on silica extraction. It was clear that the silica collected were mainly in the form of amorphous silica. Meanwhile, Sethy et al. [80] used 1 M NaOH solution to produce Na_2SiO_3 from bamboo leaf ash. A high percentage of amorphous silica nanoparticles with an average particle size of 20 nm was obtained along with a few large-sized agglomerated nanoparticles.

Fatimah et al. [81] conducted an alkaline treatment process of bamboo leaf ash to extract silica in which 4 M NaOH solution was used. Amorphous biogenic silica with a purity of 96.4% and 98 m^2/g of surface area was successfully obtained, and no impurities were detected. Jumari et al. [82], on the other hand, used 2 M NaOH for the production of Na_2SiO_3 solution from coal FA. Amorphous silica was successfully obtained with a diameter of ~7.5 μm consisting of clustering sub-micron-sized primary particles, small adherents on the surface, and NaCl impurities in the sample. This occurred as a result of an incomplete cleaning process or salt that was trapped in the silica matrix.

The impact of reaction temperature on silica extraction is also important to consider, particularly in terms of yield, purity, crystallinity, and surface area of the silica product. Park et al. [83] evaluated the performance of silica extraction at six different alkaline reaction temperatures (25 °C, 60 °C, 70 °C, 80 °C, 90 °C, and 100 °C) and found that only a small amount (1.4–14%) of silica leached from the rice husk into the NaOH solution at 25 °C. The silica yield increased to 68.4% at 60 °C. However, after reaching 70 °C, the silica yield did not improve. It can be concluded that the best reaction temperature for the alkaline solution of rice husk would be 70 °C. As a result, amorphous silica with a purity of 98.5% and surface area of 1.97 m^2/g was successfully obtained. Zhao et al. [72] also found that when the alkaline reaction temperature increased from 25 °C to 90 °C, the silica extraction rate increased from 72.13% to 81.84%. As a result, due to the high dissolving amorphous silica, the alkaline treatment was performed at a lower temperature.

Nguyen et al. [84] studied the effect of temperature on the extraction of silica nanoparticles from rice husk ash. The study was performed using a temperature ranging from 60 °C to 100 °C with an interval temperature of 10 °C. The amount of silica obtained increased with the temperature, and the maximum amount was observed around 90 °C. The amount remained the same until 100 °C. The maximum extraction mass and efficiency of silica was 1.66 g and 83%, respectively. Spherical shaped silica with a purity of 98% and a specific surface area of 78 m^2/g was obtained. However, little remaining sodium was observed due to imperfect washing. On the other hand, Dhaneswara et al. [85] treated rice husk ash with alkaline solution at a temperature of 80 °C. The extracted amorphous silica has a purity of 98–99%. However, potassium was observed to be the only impurity detected in the synthesised silica. The extracted silica has a surface area ranging from 76.75 to 236.2 m^2/g. The elimination of organic matters and impurities during the reflux process with NaOH resulted in a large surface area of the silica produced from rice husk ash.

Nayak et al. [86] conducted alkali treatment of rice husk ash using NaOH solution at 90 °C. After the alkaline treatment, a combination of small grain-like and fine particles was seen due to the formation of clusters and the highest silica product recovered from the NaOH treatment was 99.13%. The amorphous silica obtained possessed an irregular arrangement and porous network structure with a spherical form of less than 200 nm with purity ranging from 74.89% to 91.35%. The presence of mineral impurities in the silica was caused by the formation of instant gel during the neutralisation process, which entrapped Na, K, and Cl ions. Meanwhile, Alam et al. [87] conducted an extraction experiment using treated bottom ash to understand the dissolution behaviour of silica and the formation of secondary silicate species at various temperatures. Approximately 20% of the available silica dissolved at 20 °C and 75 °C, while more than 55% of silica was obtained. This is because the dissolution of silica is enhanced under non-ambient alkaline temperatures. No significant difference in the extraction efficiency was noticed upon further increasing the reaction temperature to 90 °C.

Although the effect of operating time on silica extraction does not appear to be significant, Zhao et al. [72] found that the dissolution of

silica was relatively rapid with silica extraction reaching as high as 76.46% at 30 min followed by a minor increase of 5.82% when the reaction was carried out for 5 h. Because most of the silica in the bauxite reaction residue are not wrapped with other minerals, it can be concluded that most of the silicate minerals generate silicic acid and amorphous silica is precipitated. As a result, NaOH is able to recover most of the silica. Haq et al. [88] studied the effect of operating temperature on silica extraction from rice husk ash from 20 min to 2 h. It was discovered that the yield percentage of extracted silica increased up to 90 min and then remained constant.

Yadav and Fulekar [12] extracted silica from FA using NaOH treatment for 90 min. The presence of Si and O validated the production of silica nanoparticles from FA with particle purity ranging from 94% to 97%. The morphology of the synthesised silica was spherical and in the range size of 10–60 nm. Osman and Sapawe [89] managed to extract 68.4% of silica from oil palm frond ash after an hour of treatment. The purity of the amorphous silica obtained was 90%. Nazriati et al. [90] extracted silica from sugarcane bagasse ash using NaOH treatment for an hour. Hydrophobic silica aerogels with high surface area ranging from 450 to 1114 m^2/g and the pore volume ranging from 0.75 to 2.16 cm^3/g were successfully synthesised. Nassar et al. [6] successfully synthesised pure silica nanoparticles with controlled phase, purity and shape from rice husk ash using NaOH treatment for 45 min. Silica was extracted by dissolving it in NaOH solution and then converting it into sodium silicate solution. The amorphous silica product consisted of aggregates of two distinct morphologies (peanut and irregularly shaped particles) with an average size of 14 nm, a surface area ranging from 4.09 to 59.28 m^2/g, and an average pore diameter of 11.42–14.88 nm. The fabricated silica product was made up entirely of Si and O components, indicating that it was extremely pure. Table 3 summarises some of the synthesis parameters used by previous studies for the alkaline treatment process.

3.3. Recovery of silica

There are many methods available for silica recovery. These include CVD, hydrothermal synthesis, microemulsion technique, sonochemical technique, co-precipitation technique, and sol-gel technique. Based on the simplicity and efficiency of the process, hydrothermal, co-precipitation, and sol-gel are the most widely used techniques for the recovery of silica.

3.3.1. Hydrothermal synthesis

Hydrothermal synthesis refers to the synthesis of chemicals in a sealed and heated solution above ambient temperature and pressure [91]. During the hydrothermal process, the chemical reactions occur in a sealed and heated aqueous solution at temperatures more than 25 °C and pressure greater than 100 kPa to produce crystalline materials directly from the solution. Pressures as high as 500 MPa and temperatures as high as 1000 °C can be used in this method to improve the reactant dissolution which resulted in the nucleation and growth of certain types of materials [92].

The term "hydrothermal" comes from earth science in the nineteenth century, and it refers to a temperature and water pressure regime. The crystal growth in the artificial hydrothermal synthesis process is typically carried out in an autoclave, which is a steel pressure vessel [91]. This technique has been successfully utilised to synthesise a wide spectrum of nanomaterials. It also offers a number of advantages over other techniques such as the ability to create nanomaterials that are stable at high temperatures [93]. Different synthesis strategies for precise control of hydrothermal synthesis conditions have recently been developed to tailor synthesised product properties in terms of size, shape, and composition [92]. Internal factors related to the reaction system such as the use of organic additives, templates, and substrates, as well as external environmental effects of the use of microwaves, electric fields or magnetic fields during hydrothermal synthesis to achieve desired materials structure forms, are part of these strategies [94]. Fig. 5 shows some of the silica products synthesised using hydrothermal synthesis. Wang et al. [95] synthesised cyanofunctionalized mesoporous silica nanospheres from coal FA and the SEM image (Fig. 5 (a)) showed uniform spherical microstructure. This is because synthetic method was applied from homogeneous aqueous system to heterogeneous alkanes-aqueous system, microstructure of the material changed from irregular agglomerate to uniform spherical microstructure. Arumugam et al. [96] synthesised MCM-41 from bamboo leaf ash and observed agglomeration of primary particles into larger particles which physically resembled irregular rods (Fig. 5 (b)). The large aggregates were due to the insertion of irregular cylindrical rods in a continuous, and extensive layering among each other. On the other hand, Wang et al. [63] synthesised SBA-15 from coal gangue and the SEM image (Fig. 5 (c)) showed several spherical particles with average diameters of 2–3 μm followed by some small irregular shape particles. Other than that, Bathla et al. [97] hydrothermally synthesised silica nanowired from rice husk ash. The obtained silica had smooth morphology with no visible irregularities on the surface and it showed wire-like and web-like structure.

Different processing factors such as the type of surfactant, hydrothermal temperature, and reaction time influence the porosity and morphology of the synthesised silica. The employment of surfactants in the synthesis of silica materials has long been known to impact important material characteristics including pore diameter, structural order, and phase behaviour [98]. Liou et al. [99] prepared SBA-15 through hydrothermal treatment using a surfactant mixture of P123 and HCl. The isotherm of the silica produced was type IV isotherms, which is related to hysteresis type H1 that indicates the production of slit-like mesopores in the material was based on the pore structure analysis. According to

Table 3
Previous studies on extraction of silica using different alkaline treatment parameters.

Raw material	Investigation parameters			Silica properties produced			Reference
	Concentration (M)	Temperature (°C)	Duration (h)	Purity (%)	Crystallinity	Surface area (m^2/g)	
Sugarcane bagasse ash	2	Reflux	1	98.92	Amorphous	240	[14]
Bauxite reaction residue	1, 2, 3, 4, 5	45, 60, 75, 90	0.5, 1, 2, 3, 5	81.45	Amorphous	–	[72]
Bamboo leaf ash	1	80	2	–	Amorphous	–	[80]
Bamboo leaf ash	4	105	4	96.4	Amorphous	98	[81]
Coal fly ash	2	90	4	~ 94	Amorphous	–	[82]
Rice husk	0.1, 0.15, 0.2, 0.5, 1	25, 60, 70, 80, 90, 100	1, 2, 3, 4, 5	98.5	Amorphous	1.973	[83]
Rice husk ash	2, 2.5, 3.0, 3.5, 4	60, 70, 80, 90, 100	1, 1.5, 2, 2.5, 3	98	–	78	[84]
Rice husk ash	–	80	1	98–99	Amorphous	76.75–236.2	[85]
Rice husk ash	1	90	2	74.89–91.35	Amorphous	–	[86]
MSWI bottom ash	–	20, 75, 90	24, 48, 72	98.5	Amorphous	870	[87]
Rice husk ash	0.4, 0.6, 0.8, 1.0, 1.2	Reflux	0.5, 1, 1.5, 2	–	Amorphous	–	[88]
Fly ash	8	95	1.5	94	Amorphous	–	[12]
Oil palm frond ash	2	Ambient	1	~90	Amorphous	–	[89]
Sugarcane bagasse ash	2	Boil	1	–	Amorphous	450–1114	[90]
Rice husk ash	2	Reflux	0.75	–	Amorphous	4.09–59.28	[6]

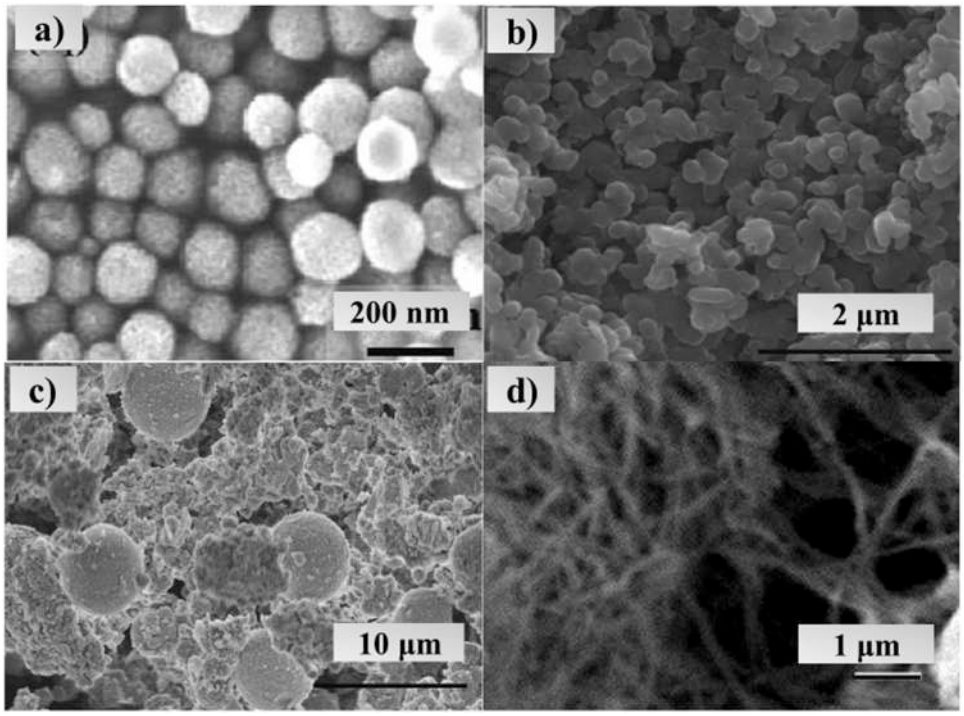

Fig. 5. Scanning electron microscopy images of silica products synthesised using hydrothermal method: (a) mesoporous silica nanosphere from coal fly ash [95]. (b) MCM-41 from bamboo leaf ash [96]. (c) SBA-15 from coal gangue [63]. (d) silica nanowires from rice husk [97].
(a) Reprinted with permission from Elsevier, (b) Reprinted with permission from Springer Nature. (c) Reprinted with permission from Elsevier. (c) Reproduced from Hindawi. (d) Reprinted withpermission from Springer Nature.

the pore distribution, the silica obtained contained large mesopores with a centre diameter of 6.34 nm. The silica had a pore volume of 0.876 cm^3/g and a specific surface area of 472 m^2/g. The silica particles obtained had a mesopore fraction of 100%. The aggregated silica particles were 0.33 µm wide, which is normal for SBA-15. A large-scale hexagonal mesostructure of silicate compounds and self-assembled surfactant micelles was seen in the silica. The average mesoporous diameter was 6.5 nm, which was close to the pore size analysis value.

Fatimah et al. [100] utilised cetyl trimethyl ammonium bromide (CTAB) as the surfactant for the synthesis of silica. The silica produced from the bamboo leaf ash had a broad peak XRD spectra at $2\theta = 22^{\circ}$, which corresponded to the amorphous silica. The silica had a purity of 98.92% and was found to have a random rough surface with mostly between 10 and 40 nm in size. The existence of cubic nanostructures and irregular spherical particles is indicated by the irregular shapes, which are consistent with the SEM profile. Meléndez-Ortiz et al. [98] studied the effect of co-surfactant in the synthesis of mesoporous silica material of MCM-41. The XRD analysis confirmed that the 2-propanol anhydrous (i-PrOH) produced a well-ordered mesoporous MCM-41 silica. Aside from that, the sample produced from butanol (BuOH) only had a wide peak (plane 100) with low values of 2θ, while the peaks for the (110) and (200) were absent due to a disordered silica structure. This behaviour may be explained by the fact that the amount of condensation decreases as the number of carbon atoms in the co-surfactant chain increases. As a result, better ordered mesoporous silica was produced with greater condensation rates. In addition, the MCM-41 sample from BuOH had the greatest ᴅ-spacing value. When the length of the alcohol chain increases, the thickness of the amphiphilic bilayer of the surfactant phase increases.

Besides the type of surfactants, hydrothermal temperature also plays an important role in the properties of the synthesised silica. Sun et al. [101] used an autoclave to hydrothermally treat a CTAB:Ethanol:TEOS combination at 140 °C or 180 °C for 24 h. Adjusting the parameters of the synthesis mixture resulted in an excellent monodispersity MSNs with particle sizes ranging from 90 to 400 nm, nanopores of 7.4–15.7 nm and surface area over 500 m^2/g. Arumugam et al. [96] produced MCM-41 using a hydrothermal route at 100 °C. The prepared MCM-41 have a specific surface area of 1096 m^2/g, an average pore diameter ranging from 2.91 to 3.65 nm, and particle sizes ranging from 300 to 500 nm.

Bai et al. [102] evaluated the effects of hydrothermal temperature on the characteristics of the synthesised SBA-15 materials. As the hydrothermal temperature increased, the total specific surface area of the SBA-15 initially increased from 726.91 at 100 °C to 755.07 m^2/g at 120 °C, then progressively decreased from the maximum value of 755.07 m^2/g at 120 °C to 307.03 m^2/g at 180 °C with a total reduction of 60%. It was also discovered that when the temperature was increased, the average pore size increased steadily from 5.26 to 14.09 nm. This is in line with the calculated pore size values.

Finally, the textural properties of the produced silica are also influenced by the synthesis periods of the precipitation and the hydrothermal treatment stages. The effect of hydrothermal treatment time on the textural characteristics of SBA-15 produced was investigated by Juárez-Serrano et al. [103]. The synthesised silica displayed thicker and less well-formed sticks when no hydrothermal treatment was performed as seen in the SEM pictures. As time was extended, well-formed sticks of increasing size and length were detected resulting in larger particles as shown in Fig. 6. The characteristics of silica obtained at intermediate hydrothermal treatment periods of 6 and 15 h were similar, while the silica prepared after 24 h showed an increase in the Brunauer-Emmet-Teller (BET) surface area, external surface area, specific pore volume, and average pore size. Furthermore, silica without the hydrothermal treatment had the smallest pore size of 4.9 nm. The XRD data revealed that when the hydrothermal treatment period increased, all planes moved to lower values of 2θ, causing an increase in the intensity and the definition of the (110) and (200) peaks. The findings indicated that more ordered materials were produced.

Majchrzak-Kucęba and Nowak [104] produced MCM-41 using the hydrothermal method at 100 °C for 48 h. The MCM-41 obtained had a specific surface area ranging from 170 to 610 m^2/g, average pore diameter ranging from 3.9 to 6.2 nm, and particle sizes in the range of 3–200 μm. Meanwhile, Tolba et al. [105] obtained amorphous nanosilica with particle size ranging from 10 to 50 nm via hydrothermal synthesis at 160 °C for 2 h. Table 4 shows the previous studies done on the production of silica via hydrothermal synthesis.

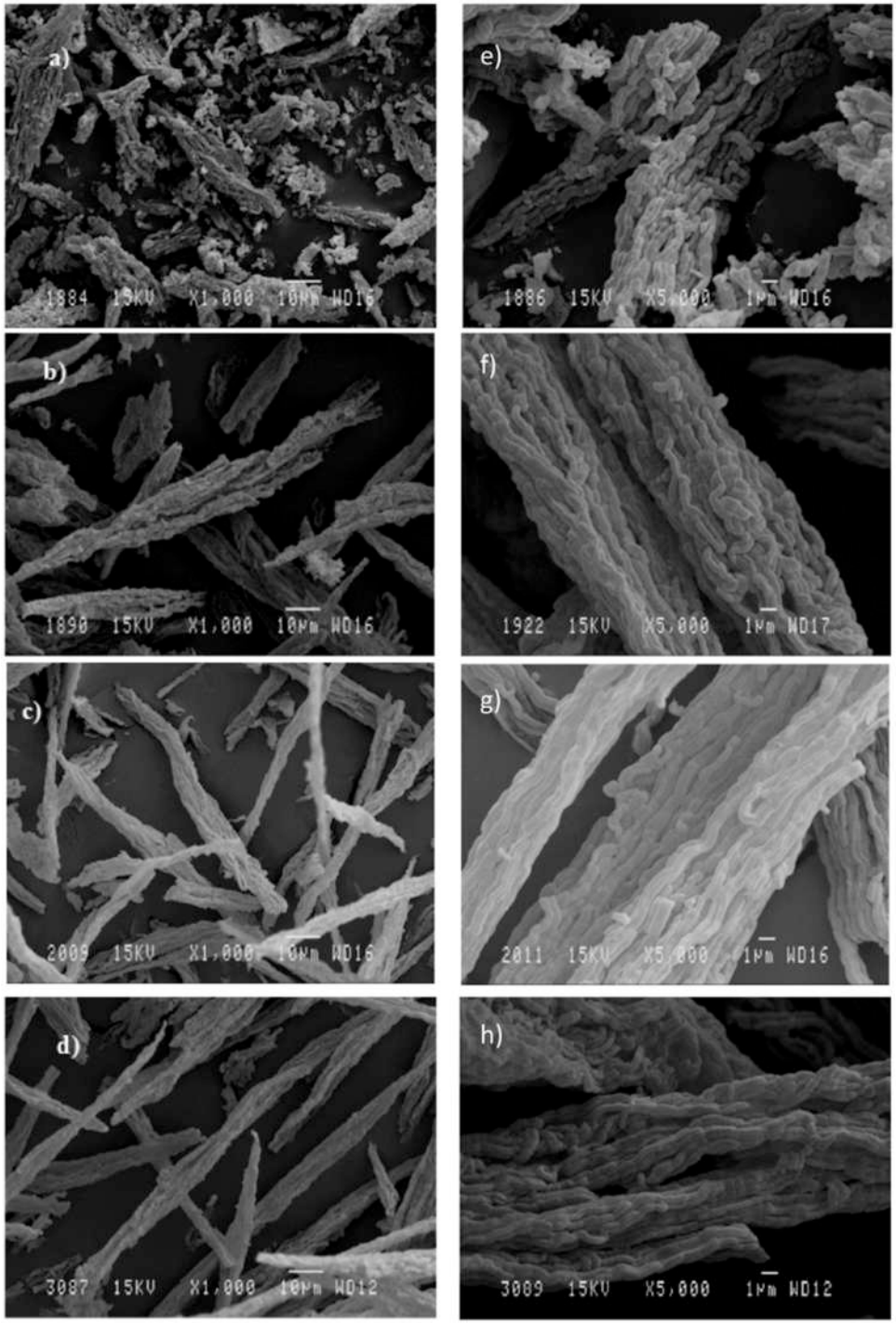

Fig. 6. SEM images of the silica obtained at different hydrothermal treatment times and magnifications: (a,e) no treatment, (b,f) 6 h, (c,g) 15 h, and (d,h) 24 h [103]. Reproduced from MDPI.

3.3.2. Co-precipitation technique

Co-precipitation is a method to obtain a uniform composition in two or more cations homogenous solution using precipitation reaction. It is one of the most significant ways for the synthesis of composites comprising two or more metal elements [49]. In the co-precipitation reaction, nucleation, growth, coarsening and agglomeration processes occur simultaneously [48]. This process, much like sol-gel begins with a solution, involves dissolving the starting components in a common solvent before adding a precipitating agent to create a homogenous and a single-phase inorganic solid. Then, the precipitate can be dissolved at a high temperature to get the desired mixed oxide material. Co-precipitation also helps keep the necessary cations close together in the reaction medium and decreases the decomposition temperature. Simple metal salts that dissolve easily in water or other suitable solvents can be used as starting materials. It is one of the most used techniques in producing nanoparticles [47].

One crucial parameter that determines the characteristics of the final product is the precipitant concentration. Hasanah et al. [113] extracted silica particles from volcanic ash using this method. The sodium silicate obtained from the volcanic ash was titrated with 2 M HCl. The precipitated gel was separated from the solution and dried in an oven at 70 °C to 80 °C. The white silica compounds obtained had a composition of

Table 4
Previous studies on the production of silica using different hydrothermal synthesis parameters.

Reference	Investigation parameters			Silica properties obtained		
	Surfactant	Temperature (°C)	Duration (h)	Particle size (nm)	Surface area (m^2/g)	Pore diameter (nm)
[101]	CTAB	140	24	90–400	502	7.4 – 15.7
[99]	P123	100	24	330	472	6.5
[100]	CTMA	–	Overnight	10–40	–	–
[96]	CTAB	100	24	300–500	1096	2.91 – 3.65
[104]	CTAB	100	48	$1 \times 10^3 - 2 \times 10^5$	170–610	3.9 – 6.2
[105]	–	100–800	1 – 5	10–50	–	–
[98]	i-PrOH, BuOH	80	72	2–3	860 – 1028	2.38 – 2.50
[106]	–	170	–	100–300	–	–
[107]	CTAB	100	48	250	1060	2.89
[108]	PP	100	2	–	134	–
[102]	P123	100, 120, 140, 160, 180	24	5.29–14.09	307.03 – 775.07	5.58 – 11.20
[109]	Pluronic F-127	100–200	1, 2, 4	–	290.4 – 677.3	12.2 – 15.6
[110]	P123, 1-butanol	60, 90, 120, 150	0, 12, 18, 24, 48, 72	–	665–858	4.2 – 9.1
[43]	P123, butanol	100	24	–	432–636	6.0 – 7.2
[103]	P123	80	0, 6, 15, 24	–	728–930	3.8 – 6.2
[111]	–	300	1	–	703.2	–
[112]	Pluronic F-127	Ambient	24	20–30	201–497	3.6 – 5.3
[97]	Edamine solution	200	120	15–35	–	–

48% and granules-like shape with a pore size that was large enough to form uneven distribution of globules as shown in Fig. 8(a). The silica extracted also had low stability possibly due to the high content of Cl impurities, and it possessed amorphous characteristics. Indrasti et al. [114], on the other hand, synthesised nanosilica from boiler ash using the precipitation method. Sodium silicate from the boiler ash was added with 5 N H_2SO_4 followed by 2.5 N NH_4OH. The solution was dried at 105 °C for 12 h. The silica obtained was further hydrolysed using acid and filtered followed by a washing step. The residue was dissolved again in NaOH and titrated with H_2SO_4. It was finally dried at a temperature of 105 °C for 12 h. The nanosilica obtained had a particle size ranging from 214.04 to 698.24 nm and possessed a polygonal morphology.

Besides the precipitant concentration, the pH of the solution also plays an important role in order to control the morphology, size, crystallinity, and size distribution of the silica produced. Ngoc et al. [115] prepared high-purity amorphous silica from rice husk using this method in which HCl was added to the sodium silicate solution obtained from rice husk until the solution's pH reached 4 and white amorphous precipitate was formed in the solution. The precipitate was filtered and washed with distilled water. It was then dried at 110 °C for 3 h. The silica powder obtained formed aggregates of primary particles (about 25 nm) and a BET surface area of 68.22 m^2/g. Research on the synthesis of silica nanoparticles co-precipitation method has also been reported by Silvia and Zainuri [116]. Sodium silicate solution obtained from silica sand was titrated with 2 M of HCl until the pH reached 7 and gel formation was observed. The silica gel obtained was filtered and washed until the pH was neutral. Amorphous silica was obtained with a particle diameter of 25 nm. Nurbaiti and Pratapa [117] also reported the synthesis of cristobalite from silica sand. The sodium silicate obtained from silica sand was titrated with 2 M HCl to form silicic acid. The gel was then dried at 100 °C resulting in amorphous silica powder. Table 5 shows the previous studies done on the production of silica via the co-precipitation technique.

3.3.3. Sol-gel technique

Sol-gel process involves the formation of mineral phases starting from soluble molecular precursors following an inorganic polymerisation reaction [118]. The reaction is carried out at room temperature, in water or organic solvents, and in a wide range of pH or ionic strength conditions. The "sol-gel process" takes its title from the transition of a liquid (solution or colloidal solution) to a solid (di- or multiphase gel). The reaction has been frequently utilised to make porous nanomaterials with well-defined structures, complex shapes, and a high specific surface area [119]. It is a versatile means of obtaining inorganic and organic-inorganic networks such as glasses, ceramics, films, and powders. The sol-gel method is simple and allows for precise control of component distribution in molecules by pre-orienting the network [120]. This method does not require expensive chemicals and high synthesis temperature; hence, the cost of silica production using this method is cheaper compared to other methods.

In general, this method is based on metal alkoxide or metal oxide solution hydrolysis and condensation. The hydrolysis stage produces a colloidal solution known as sol, which is then transformed into a semi-solid phase by the condensation process known as scenariosgel. To obtain the required nanoparticles, this gel is dried at a high temperature [42]. The utilised solvent and the addition of the reaction process are the primary distinctions between each synthesis method and the sol-gel technique [119]. The silica nanoparticles are obtained using the following reactions:

TEOS in a basic solution of water and alcohol [121].

$$Si(OEt)_4 + 4H_2O \rightarrow SiO_2 + 2H_2O + 4EtOH \quad (3)$$

Sodium silicate in an acidic solution of sulfuric acid [78].

$$Na_2SiO_3 + H_2SO_4 \rightarrow \quad SiO_2 + \quad Na_2SO_4 + \quad H_2O \quad (4)$$

A number of acids can be used for sol-gel technique such as HCl [122], H_2SO_4 [41], $C_6H_8O_7$, $C_2H_2O_4$ [123], HNO_3 [124,125], and CH_3COOH [126]. The type of acid used significantly influences the

Table 5
Previous studies on the production of silica using different co-precipitation parameters.

Reference	Investigation parameters			Silica properties produced		
	Precipitant	Concentration (M)	pH	Purity (%)	Particle size (nm)	Crystallinity
[113]	HCl	2	6–7	48	–	Amorphous
[114]	H_2SO_4 NH_4OH	2.50.5	7–10	44.26	214.04 – 698.24	Crystalline
[115]	HCl	0.1	4	55	~25	Amorphous
[116]	HCl	2	7	–	~25	Crystalline with amorphous background
[117]	HCl	2	–	–	–	Amorphous

hydrolysis and condensation rate, thus affecting the reaction mechanism of the sol-gel synthesis [127]. It also affects the pore structure of the silica product [128]. Liang et al. [122] produced biosilica nanoparticles from biomass powerplant FA using acid leaching treatment, alkaline treatment, and sol-gel method. HCl was used as the acid type for the sol-gel synthesis. The purity of the silica produced reached a maximum of 95.63%, and the ash was effectively transformed to an amorphous state. The hydroxyl groups in the amorphous silica were abundant indicating that the network might be converted into a linear structure with hydrogen bonds. Sphere-like and mesoporous silica nanoparticles with particle size ranging from 20 to 40 nm, BET surface area of 115 m^2/g, pore volume of 0.13 cm^3/g, and pore size of 3 nm were successfully obtained.

Aphane et al. [129] prepared silica nanoparticles from coal FA using the same method as Liang et al. [122]. However, H_2SO_4 was used as the acid for the sol-gel synthesis and high-level purity of up to 99.3% of amorphous silica nanoparticle was obtained. The particles were observed to possess mesoporous spherical shape with particle size less than 200 nm that was aggregated to form micron-size agglomeration, while surface areas exceeding 500 m^2/g, pore volume of 0.4 cm^3/g, and pore size of 2.5 nm were successfully obtained. When compared to HCl, H_2SO_4 as the acid type resulted in larger particle size and smaller pore volume of silica. With the growing concern on environmental and safety issues, efforts have been made to replace dangerous strong acids with organic acids. Terzioğlu et al. [127] titrated a silicate solution obtained from rice hull ash using HNO_3 and $C_6H_8O_7$ separately and found that the surface area of silica aerogels prepared in the presence of $C_6H_8O_7$ was found to be greater than those formed in the presence of HNO_3 at the same gelation pH. The extracted silica aerogels had a BET surface area ranging from 238 to 726 m^2/g. The mesopore fraction of $C_6H_8O_7$ gelated aerogels was greater than that of HNO_3 gelated aerogels, having pore sizes ranging from 3.24 to 10.22 nm.

Liou et al. [123] found that the yield of silica using $C_6H_8O_7$ and oxalic acid ($C_2H_2O_4$) was higher compared to HCl or H_2SO_4. However, the remaining Na concentration was higher when $C_2H_2O_4$ or $C_6H_8O_7$ was used in the precipitation procedure. Dhaneswara et al. [85] evaluated the silica synthesis performance of HCl and acetic acid (CH_3COOH). Rice husk yielded amorphous silica with a purity of 98–99%, particle sizes ranging from 9 to 12 nm, and average pore diameters ranging from 8.4 to 15 nm. The silica recovered from rice husk by HCl acidification exhibited the highest purity and surface area (236.2 m^2/g).

Besides acid type, the concentration of the acid also plays a vital role in affecting the silica extraction efficiency. Higher efficiency can be achieved by manipulating the acid concentration. Yadav and Fulekar [12] precipitated the silica using HCl with a concentration of 1–2 M. It was possible to extract amorphous silica nanoparticles with sizes ranging from 20 to 70 nm from waste FA. The produced silica nanoparticles were spherical in shape and clumped together to form a cluster. The FTIR results indicated that the major groups found in the silica were siloxane and silanol. Peaks for Si, O, C, and Na were observed in the EDS spectra of as-synthesised silica. The presence of Si and O indicates silica formation. The presence of Na, on the other hand, is due to the impurities associated with poor washing while C is related to fly ash carbon and adhesive tape. The purified final silica only had peaks for Si, O, and C; indicating that the silica purity was between 94% and 97%. After calcination and purification of the silica particles, the Si content increased dramatically while the carbon content plummeted.

In the acidification process, Manchanda et al. [130] titrated sodium silicate solution with 1 M HCl solution. Precipitation of silica particles was observed when mineral acid was used to acidify the sodium silicate solution, silicon hydroxide species condensed together to form siloxane bonds (Si-O-Si bonds) (Fig. 7 (a)). XRD analysis revealed that amorphous silica was absence of any ordered form of cristobalite silica. The silica particles were uniformly distributed, spherical, and globular in shape. The lack of a regular geometry indicates the product's amorphous nature. The particles observed an average diameter ranging from 10 to

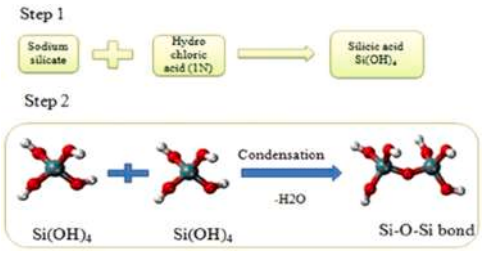

Fig. 7. Mechanism of silica particles formation from (a) coal fly ash [130]. Reprinted with permission from Springer Nature.

30 nm with minimal agglomeration. The ultra-purity of the silica product was validated by EDX analysis with Si and O making up 99.9% by weight. Yuan et al. [131] utilised 2 M HCl solution to titrate sodium silicate produced from coal FA. A type IV isotherm was seen in the Ni physisorption measurement, indicating the presence of a characteristic mesoporous structure of silica. The obtained material had an irregular form and a worm-like mesostructured. The pore distribution was found to be broad with a pore diameter centring at 3.9 nm and an average pore diameter of 4.9 nm.

It must be noted that the pH of the solution plays a huge role in the sol-gel synthesis of silica. The structure and properties of the silica product are greatly influenced by the gelation pH. This is because condensation processes are favoured and hydrolysis reactions are limited under alkali conditions in which the particles produced are less in number but bigger and denser than those created under acidic conditions [127]. Mermer and Piskin [132] studied the effect of gelation pH on the structure of the synthesised silica. According to the findings, pH 9 had the lowest density, which also means higher porosity. The density of the synthesised aerogel was between 0.276 and 0.285 g/cm^3. The XRD analysis revealed that the silica aerogel produced had an amorphous structure. The isotherms demonstrated that the aerogels were of type IV, indicating that they were mesoporous. The surface areas were measured between 338 and 943 m^2/g.

On the other hand, De Oliveira et al. [133] found that at pH 7, a more ordered structure and a higher surface area and pore volume were found to lead an adsorbent with good efficiency. At pH 13, the formation of microporous crystalline structures was favoured. Simatupang et al. [134] used 3 M HCl solution to titrate sodium silicate solution until the solution was neutral. At pH 14, the formation of silica precipitates was observed. However, at pH 8–10, the gel began to form precipitates. At pH 7, the addition of HCl acid wass topped. The silicic acid produced during the synthesis of the silica gel exhibited polycondensation to form dimers, trimers, and polymers of silicic acid by releasing water molecules in the process. The amorphous nature of the silica was confirmed using XRD analysis. The silica gel had an average pore radius of 0.015 nm, a total pore volume of 290 mL/g, and a surface area of 374 m^2/g, indicating that it was micropore.

Furthermore, by incorporating additives into the sol-gel synthesis, the porosity of the synthesised silica can be altered; hence, reducing the aggregation phenomena. In a study done by Aphane et al. [129], sodium silicate was added slowly into the polyethylene glycol (PEG) solution before gradually adding the acid solution to initiate the hydrolysis-condensation reaction. The amorphous silica obtained possess mesoporous spherical shape with a particle size of less than 200 nm, which aggregated and formed micron-size agglomeration with surface areas exceeding 500 m^2/g, pore volume of 0.4 cm^3/g, and pore size of 2.5 nm. Terzioğlu et al. [127], on the other hand, added pre-treated silica gel into a TEOS:ethanol solution before washing and drying the gel. The silica aerogel's surface area ranged from 238 to 726 m^2/g with a pore size of 3.24–10.22 nm. High mesopore fractions were also observed with a density ranging from 0.273 to 0.849 g/cm^3 and porosity ranging from 61.23% to 87.53%.

Besides the mentioned additives, Mao et al. [135] added cetyl

trimethylammonium bromide (CTAB) and n-butanol into the sodium silicate before slowly adding the acidic solution. T presence of CTAB created a physically adsorbed layer surrounding the silica nanoparticles due to the adsorption of the CTAB's positive charge heads on the silica surface. As a result, this behaviour protects silica nanoparticles from aggregating by preventing hydroxyl group interactions between silica nanoparticles and between silica and water. The silica particles dispersed fully in the water phase at lower CTAB concentrations; however, there was considerable aggregation because the CTAB molecules did not coat evenly on the silica surface. In the n-butanol phase, silica nanoparticles were shown to disperse homogeneously as the concentration rose. However, when the CTAB concentration got higher, the silica nanoparticles dispersed in n-butanol and aggregation phenomena occurred in the interfacial region between the n-butanol and water phases. This is because high CTAB concentrations cause the formation of bilayer self-arranged micelles.

Ageing temperature can also affect the surface area of the silica produced. According to Liou et al. [123], rising the ageing temperature from 20° to 50°C increased the surface area of the silica produced which leads to the rapid growth of the silica framework. The surface area decreased when the ageing temperature was increased from 50° to 120°C because the gelation rate was faster at higher formation temperatures. Pore shrinkage occurred as a result of the thicker silica framework formed and this led to a smaller surface area. Utama et al. [41] aged the solution at 90 °C and discovered that the microstructure of the amorphous silica recovered was identical to the commercially available silica. Both silicas' main particles were uniform and had a spherical particle shape with sizes in a nanoscale. Commercial silica, on the other hand, has a lower primary particle size compared to the silica obtained. The resulting silica has a BET surface area of 53.59 m^2/g, which is comparable to the commercial silica. It can be concluded that the silica produced is equivalent to the commercially available silica.

Mao et al. [135] also compared the effects of ageing temperature on silica particle formation. Due to the predominance of precipitation over dissolution processes, the silica particles produced at low temperatures of 30 °C have a particle diameter of greater than 100 nm. It was also noticed that minimal interactions between the silica surface and the additive employed were thought to be the cause of small silica particle aggregation. At 60 °C, a great uniformity and reduced size of silica particles were achieved. This is due to the fact that the state of equilibrium between the dissolution and precipitation processes correlates with the increased interactions between the hydroxyl groups on the silica surface and the additive employed. However, at 90 °C, substantial desorption of the additive was detected, resulting in an increase in particle size compared to 60 °C.

The formation of silica particles is a reversible process whereby both the dissolution and precipitation processes simultaneously happen during the ageing step. The equilibrium state between these processes could be also controlled by changing the ageing time [135]. The performance of various ageing times on the sol-gel synthesis of silica was also compared by Liou et al. [123]. It was discovered that raising the ageing period from 1 h to 12 h resulted in a significant increase in the silica surface area. The surface area decreased as the ageing period increased from 12 to 96 h. It was also noted that the ageing time has an impact on particle nucleation and surface growth. Nucleation was mostly caused by a small amount of silica precipitates that was formed in the acidic solution at the start of the reaction. As a result, the surface area of the silica was not high enough. When the ageing duration was prolonged to more than 12 h, surface development limited the silica formation. As a result, the particle size of the silica produced increased. The silica surface area was greatly reduced due to the low probability of nuclei increasing continuously.

Finally, Mao et al. [135] discovered that the phenomenon of increasing silica obtained with the increase of the ageing period was insignificant. Due to the equilibrium state of the dissolution and precipitation processes, excellent uniform size of silica particles was achieved at an ageing period of 8 h when compared to other ageing times. Unfortunately, the silica particles tended to agglomerate after 16 h of ageing resulting in high particle size. Table 6 shows the previous studies done on silica extraction from waste via the sol-gel method.

The dimensions and morphologies of the resultant materials are influenced by the sol-gel chemistry parameters such as temperature, water content, pH, surfactant or copolymer properties, and silica concentrations and sources. As a result, manipulating these factors enable the development of silica at various size, mesostructure, and morphology [5]. The modification of the sol-gel technique allows for the preparation of a wide range of porous inorganic materials that may be utilised in many applications including chromatography and catalysis [143]. In sol–gel chemistry, pH is extremely important. The ultimate aerogel structure is heavily reliant on hydrolysis and condensation processes, both of which are influenced by pH [144]. Hydrolysis is strongly favoured in an acidic environment in which molecules undergo oligomerisation reactions and form linear or random chain structures composed of Si-OH groups. On the other hand, condensation dominates in a basic environment resulting in branching networks of Si-(O-Si) with high stiffness and stability [120,144]. Furthermore, the pH value significantly impacts silica dissolution and reprecipitation whereby greater pH levels offer more porous structures due to the higher solubility. In contrast, lower pH levels offer dense and fine porous structures due to the lower dissolution [144].

Terzioğlu et al. [145] studied the effects of acid type and gelation pH on the silica aerogel properties. The surface area of silica prepared in the presence of citric acid was greater than that of silica prepared in the presence of nitric acid at the same gelation pH whereby the BET surface area decreased as the gelation pH for acids increased. Citric acid gelated aerogels had a greater mesopore fraction than nitric acid gelated aerogels. As a result, aerogels made under alkaline conditions had larger pores and a lower surface area than those made under acidic conditions. It was also discovered that silica aerogels with a higher gelation pH had a lower density. According to Rahman and Padavettan [26], more than half of the Si atoms were present on the surface of silica nanoparticles were smaller than 5 nm. As a result, one or more silanol groups (≡Si-OH) should be present on the surface. Therefore, the degree of chemical modification of silica is determined by the number of silanol groups per gram of silica. The concentration of silanol groups rises as the particle size decreases proportionally to the specific surface area. However, the fact that the quantity of silanols decreases as the particle size decreases implies that these nanoparticles may be chemically reactive and ideal for catalytic applications. Ceramic nanoparticles have a greater ability to chemically bind and even dissociate a range of hazardous organic compounds than their conventional and commercial counterparts. The increase in surface area at the nanoscale is directly connected to this unique adsorption property.

Haque et al. [143] used a sol-gel technique with various acids and solvents to produce ultrafine silica nanoparticles with dimensions of 2–6 nm. From the photoluminescence spectrophotometer (PL) investigation, silica nanoparticles were produced with formamide and HCl was observed to have spherical shape with greater crystallinity and well-defined boundaries. Additives can improve aerogels' structural and morphological properties without affecting their original features. The most favoured method is to use additives containing organic entities, surfactants, and cross-linking agents in the chemical treatment. Polyethylene glycol (PEG) is the most reliable and conventional additive for aerogel synthesis. However, it has been replaced with isocyanate or di-isocyanate, which has higher solubility and reactivity with silanol groups resulting in increased strength, density, and porosity. Additives also serve as modifying agents and could play roles such as limiting shrinkage, reducing capillary tensions, and preventing crack formation while drying [144]. Other than that, silica nanoparticles with particle diameters greater than 100 nm were discovered by Mao et al. [135] at low ageing temperatures. Due to the equilibrium state between dissolution and precipitation processes correlative with increased interaction

Table 6
Extraction of silica from waste via sol-gel method.

Materials	Investigation parameters						Silica properties produced			References
	Acid		pH	Additive	Aging		Purity (%)	Particle size (nm)	Pore size (nm)	
	(type)	(M)			(°C)	(h)				
Biomass powerplant fly ash	HCl	–	6–7	–	Room temperature	12	93.63	20–40	3	[122]
Electrostatic precipitators thermal powerplant fly ash	HCl	1–2	10	–	–	24	~94–97	20 – 70	–	[12]
Palm oil mill fly ash	H_2SO_4	–	8.75	–	90	1.67	93.4	–	–	[41]
Coal fly ash	H_2SO_4	0.5	4	PEG	55	Overnight	98.8 – 99.3	≤ 200	2.5	[129]
Biomass fly ash	HCl	1	4	CTAB	30, 60, 90	4, 8, 16	~43.7	20–30	–	[135]
Thermal powerplant fly ash	H_2SO_4	–	3, 5, 7, 9, 11	TMCs	25	24	–	–	–	[132]
Fly ash	HCl	2	1–4	–	–	–	–	–	–	[136]
Volcanic fly ash	HCl	3	6–7	–	–	–	–	–	0.031	[134]
Fly ash	HCl	2	7, 9, 11, 13	CTABr	–	72	> 90	–	3 – 5.29	[133]
Coal fly ash, Pulp waste	HCl	3	5	–	–	–	–	–	–	[137]
Bagasse fly ash	H_2SO_4	1.69	10	–	Room temperature	Overnight	93.3	–	–	[138]
Coal fly ash	HCl	2	–	Pluronic P123	100	72	–	–	4.9	[131]
Biomass fly ash	H_2SO_4	–	7	–	–	–	–	4×10^3 – 20×10^3	–	[139]
Bagasse fly ash	H_2SO_4 & HCl	1	7	–	–	18	92.5	–	–	[140]
Bagasse fly ash	HCl	1	7	–	Room temperature	18	–	–	0.3806	[141]
Palm oil mill fly ash	H_2SO_4	–	9	–	–	18	82	–	–	[142]
Coal fly ash	HCl	1	≤10	–	–	–	99.9	40–50	10–30	[130]
Rice hull ash	HNO_3, $C_6H_8O_7$	1	4	TEOS	Room temperature	18	–	–	3.24 – 10.22	[127]
Rice husk ash	$C_6H_8O_7$, $C_2H_2O_4$	1	3–11	–	20–120	1–96	99.48	–	–	[123]
Rice husk ash	HCl, CH_3COOH	1	7	–	–	–	98 – 99	9 – 12	8.4–15	[85]

between hydroxyl groups on the silica surface and the surfactant employed, silica nanoparticles with greater uniform and smaller size were also detected at an ageing temperature of 60 °C.

4. Mesoporous silica nanoparticles (MSNs) properties

In general, there are several types of MSNs families such as MCM and SBA. Among the members of the MCM family, MCM-41 is the most studied members. It is an amorphous silica array of unidirectional with 2D hexagonal mesopore structure that possessing a huge surface area larger than 1000 m^2/g and average pore diameter in the range of 2–20 nm [146]. Other MCM family members such as MCM-48 has a cubic structure, whereas MCM-50 has a lamella-like structure [4]. SBA-15 and SBA-16 are among the members of the SBA family that have been widely investigated for various applications. SBA-15 has a well-ordered and regular 2D hexagonal architecture with

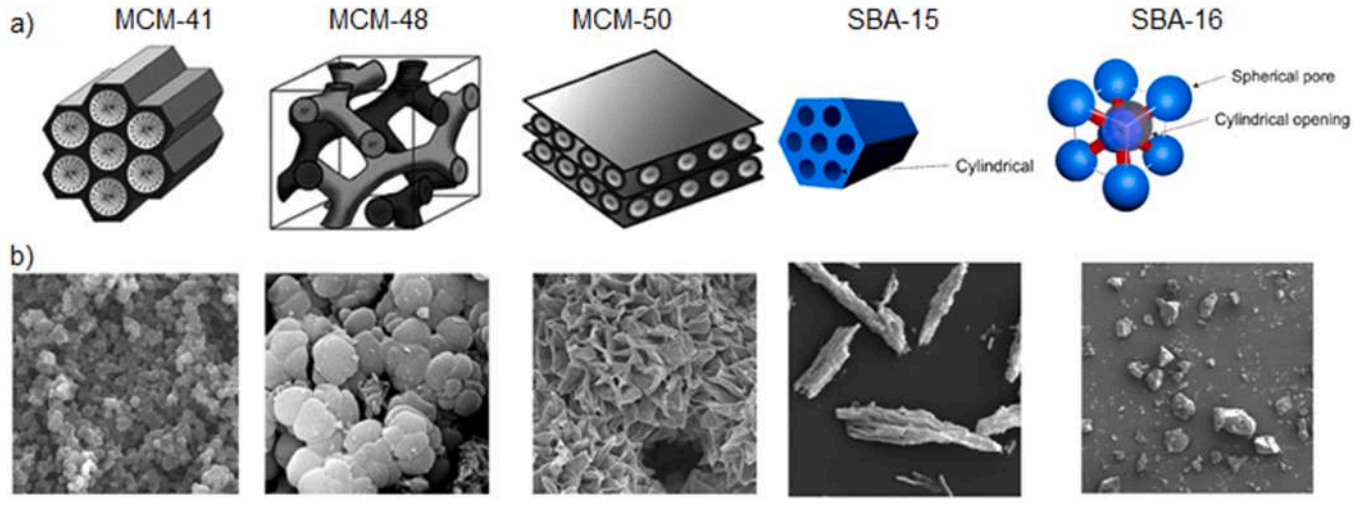

Fig. 8. (a) Structure of MCM-41, MCM-48 and MCM-50 [149] (b) SEM images of different MCMs (MCM-41 [151].
(a) Reprinted with permission from Royal Society of Chemistry and and SBA-15 and SBA-16 [150]. Reproduced from Frontiers. (b) Reprinted with permission from Elsevier, MCM-48 [152]. Reproduced from MDPI and MCM-50 [153]. Reprinted with permission from Royal Society of Chemistry) and SBAs(SBA-15 and SBA-16) [150]. Reprinted with permission from Elsevier..

interconnecting micropores, larger pore size or diameter ranging from 2 to 30 nm, high pore volume of up to 2.5 cm^3/g, large surface area of 600–1000 m^2/g, and outstanding hydrothermal stability [147,148]. In comparison, SBA-16 exhibits a complex 3D array of well-ordered mesoporous channels with cage-like architecture in a cubic body-centred symmetry [146]. Fig. 8 compares the structures and SEM images of MCM-41, MCM-48, MCM-50, SBA-15 and SBA-16.

4.1. Physical properties

Silica has a molecular weight of 60.08 g mol^{-1} and a density of 2648 g/cm^3 [154]. It has four oxygen atoms around the core Si atom, where the spatial atom of Si exhibits tetrahedral coordination. Controlling the particle size, surface area, aggregation behaviours and morphology of silica are vital, since large particle size and irregular morphologies limit the applications. Table 7 shows typical physical properties of silica including particle size, specific surface area and morphology produced from various waste sources and chemical methods. In general, it can be seen that the final particle size and surface area of silica depends on the silica source and method of synthesis. Yadav et al. [12] synthesized spherical shaped silica nanoparticles (20–70 nm) from FA using sol-gel method and observed that the morphology of the silica nanoparticles remained intact even after acidic treatment or purification. Donphai et al. [155] used hydrothermal method to synthesis MCM-41 from bagasse heavy ash and the FESEM and FETEM images indicated that the MCM-41 was finely dispersed with cluster sizes of approximately 200–300 nm and BET surface area of 1022 m^2/g.

Porous silica tends to have higher surface area which makes it more desirable due to high demands in many sectors and industries. Chandrasekar et al. [156] synthesized hexagonal and cubic mesoporous silica from powerplant bottom ash via hydrothermal method. SEM images of the synthesized MCM-41 showed that the particles have a chip-like morphology and aggregated particles together with particle size of less than 2 μm. Meanwhile, SEM images of SBA-15 showed aggregation of both worm-like and spherical particles followed by the presence of small irregular particles due to its amorphous silica phase.

Park et al. [157] prepared mesoporous silica from bottom ash using sol-gel method. TEM images of the mesoporous silica samples showed disordered pore structures with 1D mesopores. The mesoporous silicas obtained had significantly larger mesopores and the pore structure was more disordered. This was due to the addition of swelling agents which were 1-butanol and mesitylene. Falk et al. [158] synthesized silica nanoparticles from sugarcane bagasse ash via sol-gel method. TEM images of silica powder obtained clearly indicated 3D array of nanoparticles. It is possible to observe uniform and individual nanoparticles with sizes smaller than 10 nm. High agglomeration state is favoured by the gel drying process in which the destabilization of the system favours the agglomerated state of the particles that are initially well distributed in a 3D network (gel). The values of specific surface area obtained by BET method was 124.89 m^2/g. On the other hand, Mor et al. [9] extracted spheroid nanosilica with an average diameter of 10–15 nm from processed agricultural residue using sol-gel method. The physical properties of silica material show a wide variation in accordance with their source and synthesis method. It can be concluded from Table 7 that the physical properties such as particle size and surface area of the produced silica particles depend on the operating conditions employed.

4.2. Chemical properties

The chemical properties of silica material are directly influenced by the major constituent of the waste. Several instruments have been commonly used to evaluate the crystallographic structure, chemical composition, and chemical bonds of silica. These include X-ray fluorescence (XRF), X-ray diffraction (XRD), and Fourier-transform infrared (FTIR) spectroscopy.

XRF investigation is typically performed to evaluate the chemical composition of the ash waste as a source of silica. This analysis will provide an understanding on the type of oxides and the quantity of silica available in the waste. If the quantity of silica is not high enough, it might not be economical to produce silica from the waste. XRF is also used after the synthesis of silica to confirm the effectiveness of silica extraction and to determine the quality of the silica produced. Table 8 summarises the oxides composition of silica obtained from various sources. Nurwahid et al. [159] managed to produce nanosilica from sugarcane bagasse ash with 98.4% purity and 96.3% of silica from

Table 7
Physical properties of the silica produced.

Source of silica	Method	Operating condition							Particle size	Surface area	Reference
		Surfactant	Acid	Conc.	pH	Heating temperature	Heating Duration	Aging duration			
Fly ash	Sol-gel	–	HCl	1 – 2 M	10	–	–	24 h	20 – 70 nm	–	[12]
Bagasse heavy ash	Hydrothermal	CTAC solution	HCl	1 M	6.5	100	24 h		200–300 nm	1022 m^2/g	[155]
Powerplant bottom ash	Hydrothermal	CTAB solution	Acetic acid	–	10	100	48 h	–	~ 2 μm	847–1393 m^2/g	[156]
(0.07 – 4.75 mm)	Sol-gel	P123	HCl	–	–	–	–	24 h		512 – 771 m^2/g	
				–	–	–	–	72 h	1 – 2 μm	753 – 986 m^2/g	[157]
Sugarcane bagasse ash	Sol-gel	–	HCl	1 M	7	–	–	24 h	Less than 10 nm	124.89 m^2/g	[158]
		–	HCl	1 M	7	–	–	24 h	294 nm	–	[159]
Pumice stone	Sol-gel	–	H_2SO_4	5 M	7	–	–	24 h	292 nm	–	
Rice husk ash	Sol-gel	–	HCl	1 N	–	–	–	–	10 – 15 nm	–	[9]
		–	HCl	–	–	–	–	24 h	~22 nm	–	[160]
Bamboo leaf ash	Sol-gel	–	H_2SO_4	1 – 10 N	2–3	–	–	–	3.9 – 6.2 nm	544–575 m^2/g	[161]
Silica fume (20 – 400 nm)	Hydrothermal	CTAB	Ethyl acetate	–	–	–	–	1.5 h	3 – 6 μm, 3 – 6 nm, 10 – 20 μm	557.9, 559.2, 672.8 m^2/g	[162]
Gold mine tailings slurry	Hydrothermal	P123	HCl	–	–	90–110	24 – 72 h	–	1 μm	448 – 661 m^2/g	[163]
Paddy straw	Sol-gel	–	H_2SO_4	–	6.5	–	–	–	15 – 20 nm	–	[164]
Boron waste (2 – 5 μm)	Hydrothermal	CTAB	H_2SO_4	2 M	10	105	24 h	–	Less than 200 nm	1035.534 m^2/g	[165]

Table 8
Composition of oxides in various sources and silica produced from XRF analysis.

Source	Chemical composition in the source (%)	Chemical composition of final silica (%)	Reference
Sugarcane bagasse ash	–	$SiO_2 = 98.4$ $P_2O_5 = 0.6$ $Al_2O_5 = 0.5$ Others = 0.5	[159]
Pumice stone	–	$SiO_2 = 96.3$ $P_2O_5 = 0.9$ $Al_2O_5 = 0.8$ Others = 2.0	
Sugarcane bagasse ash	$SiO_2 = 49.8$ $Fe_2O_3 = 19.3$ $Al_2O_3 = 15.6$ Others = 15.3	$SiO_2 = 96.8$ $P_2O_5 = 0.8$ $Al_2O_5 = 0.7$ Others = 1.7	[158]
Residual sand of wastewater treatment	$SiO_2 = 73.27$ $Fe_2O_3 = 5.02$ $Al_2O_3 = 6.34$ Others = 15.37	$SiO_2 = 96.35$ $Fe_2O_3 = 1.59$ $Al_2O_3 = 1.59$ Others = 0.47	[166]
Rice husk ash	$SiO_2 = 85.85$ $Fe_2O_3 = 1.04$ $Al_2O_3 = 1.86$ Others = 11.25	$SiO_2 = 96.44$ $Fe_2O_3 = 0.01$ $Al_2O_3 = 0.18$ Others = 3.37	[70]
Biomass fly ash	$SiO_2 = 44.41$ $Fe_2O_3 = 3.63$ $Al_2O_3 = 10.80$ Others = 41.16	$SiO_2 = 93.63$ $Fe_2O_3 = 0.80$ $Al_2O_3 = 1.50$ Others = 4.07	[122]
Rice husk ash	–	$SiO_2 = 94.5$ $Fe_2O_3 = 0.36$ $CaO = 1.1$ Others = 4.04	[10]
Coal fly ash	$SiO_2 = 45.15$ $Fe_2O_3 = 1.37$ $Al_2O_3 = 24.20$ Others = 29.28	$SiO_2 = 98.62$ $Fe_2O_3 = 0.01$ $Al_2O_3 = 0.13$ Others = 1.24	[129]
Coal fly ash	$SiO_2 = 33.07$ $Fe_2O_3 = 33.61$ $Al_2O_3 = 19.81$ Others = 13.51	$SiO_2 = 94.27$ $Fe_2O_3 = 0.90$ $Al_2O_3 = 3.04$ Others = 1.79	[133]

pumice stone using sol-gel method, where HCl was used to titrate silicate solution produced from bagasse ash and H_2SO_4 was used to titrate silicate solution produced from pumice stone. This purity is in the expected range of silica synthesis with very minimal contaminants (2–5%) such as phosphorus oxide, aluminium oxide, and sulphur oxide. Falk et al. [158] extracted silica nanoparticles with slightly lower percentage of 96.8%, which could be due to the shorter time of alkaline (NaOH) dissolution process that was only an hour instead of four hours. The solubility of the silica may be affected by the operating treatment time which in turn influences the silica purity. However, its purity is still considered high as HCl pre-treatment was performed on the ash. This result demonstrated that the production of silica with a purity more than 95% from waste is possible.

On the other hand, Silva et al. [166] also reported silica purity as high as 96.35%. However, this study used different method of preparing silica from waste, where the residual sand from wastewater treatment plant was first calcined and mixed with a chemical activator. The calcination step of the residual sand contributed to the increase in SiO_2 percent in the waste. Meanwhile, the addition of chemical activator, which was sodium carbonate, further decreased the metal oxides content and increased the SiO_2 purity. Steven et al. [70] managed to increase the silica content in the extracted silica from rice husk ash using an optimum experimental sequence, where the step started with an acid leaching treatment and ended with drying of the silica product. The method successfully produced high silica content from the rice husk ash. This is because the acid leaching and gel washing steps successfully remove almost all of the impurities.

Oliveira et al. [133] successfully synthesized mesoporous silica from coal FA by determining the optimum pH condition during the synthesis process. The silica produced at pH 9 was found to have the highest purity of 94.27%. This is because the properties of the silica product is greatly influenced by the gelation pH of the process, where the hydrolysis process is favoured as the pH value decreases. Therefore, more particles are produced as compared to those produced at higher pH value. It can be concluded that the purity of the silica product depends on the raw material used, pre-treatments, and the conditions applied during the synthesis.

Fig. 9 shows the XRD patterns of silica material produced from various waste source. It can be seen that the XRD pattern of agricultural and industrial waste such as sugarcane bagasse ash [158] and biomass fly ash [122] has a high crystallinity with various components such as quartz, cristobalite, and calcite. After the extraction of silica, a broad peak at the angle of $2\theta = 22^{\circ}$ appears, indicating that amorphous silica is formed [159]. The diffraction peak at 2θ of $20^{\circ} - 30^{\circ}$ is the characteristic peak of silica which is due to the disordered form of cristobalite. This peak is corresponded to the reflection from plane (110) [161]. Mor et al. [9] extracted nanosilica from rice husk ash where the extracted silica showed a wide and broad peak centred at 22°. This clearly indicated the presence of silica and the absence of other elements. The absence of any other peaks indicates the purity of the synthesized silica nanoparticles. However, the condition of silica production must me optimized in order to obtain high purity silica nanoparticle. Pallavi et al. [167] found that during acid leaching treatment, most impurities were reduced as the temperature increased. This is because at higher temperature, impurities can dissolve easily in the acid solution. Some impurities such as Al_2O_3 and P_2O_5 do not require high temperature as lower temperature is sufficient enough to remove them. However, some acids have low boiling and decomposition temperature; thus, the utilisation of high temperatures may cause the acid and water to evaporate and affecting the solubility of the impurities. This in turn adversely affects the purity of the obtained silica. Silva et al. [166] extracted porous silica from residual sand of wastewater treatment where the X-Ray diffractogram of the synthesised silica and commercial silica gel both possess amorphous characteristics. The diffractograms showed a broad peak at 2θ of 27.79°, which indicated the successful formation of an amorphous material.

FTIR analysis is typically carried out to confirm the component of silica in the sample. Fig. 10 shows the compilation of typical FTIR analysis for waste and silica produced ash, and product samples. In general, peaks at 460, 700, and 1000 cm^{-1} are attributed to the Si-O-Si bending, Si-O-Si symmetric stretching and Si-O-Si asymmetric stretching, respectively [168]. If the peaks are observed in the samples, it indicates that the samples contain silica component. In certain cases, additional peaks may be observed at 1400 cm^{-1}, which indicates C═C aromatic from the graphite (waste). Additional peak at 950 cm^{-1} could be detected owing to the presence of water molecules (OH) in the silica matrix [169]. Table 9 summarizes the typical functional groups and wavenumbers observed in ash waste and silica nanoparticles.

4.3. Thermal properties

Thermogravimetric analyser (TGA) is used to understand the thermal behaviour and thermodynamic analysis of the source of silica and synthesized silica nanoparticles, where thermogravimetric curve shows percent weight loss in relation to temperature of degradation. Fig. 11 shows the results of thermal analysis of silica derived from several sources. In general, there are three temperature zones: (1) low temperature (<100 °C) due to the physical moisture evaporation that occurs in the samples; (2) intermediate temperature (100–400 °C) which attributed to the degradation process or cleavage of carbon compounds; and (3) high temperature (>400 °C) where minimum change in mass is attained.

Kauldhar and Yadav [164] synthesised silica from paddy straw powder and the TGA curve (Fig. 11 **(a)**) showed that the amount of characteristic loss in weight was recorded up to three different stages

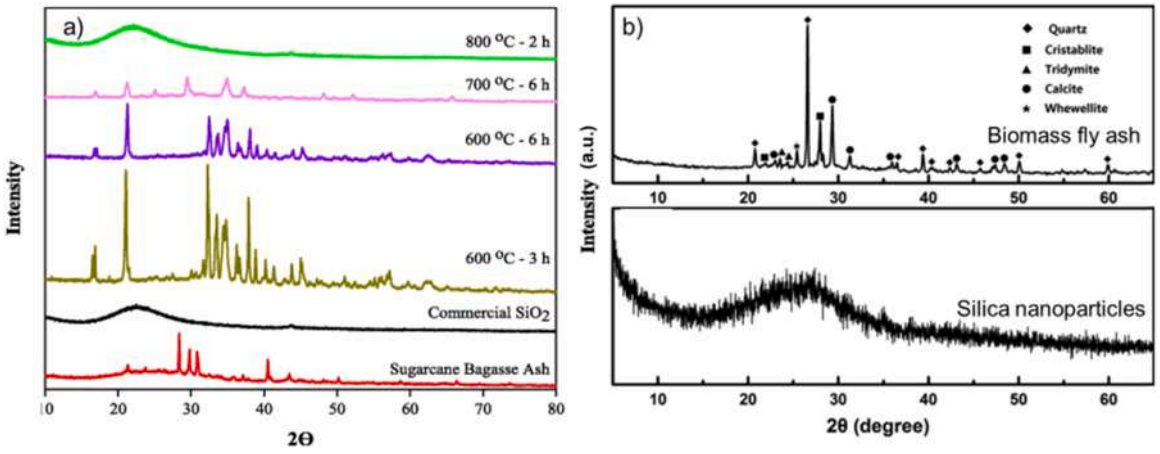

Fig. 9. (a) XRD patterns of silica material from (a) sugarcane bagasse ash [158]. (b) biomass fly ash [122].
Reprinted with permission from Elsevier and (b) Reprinted with permission from Elsevier.

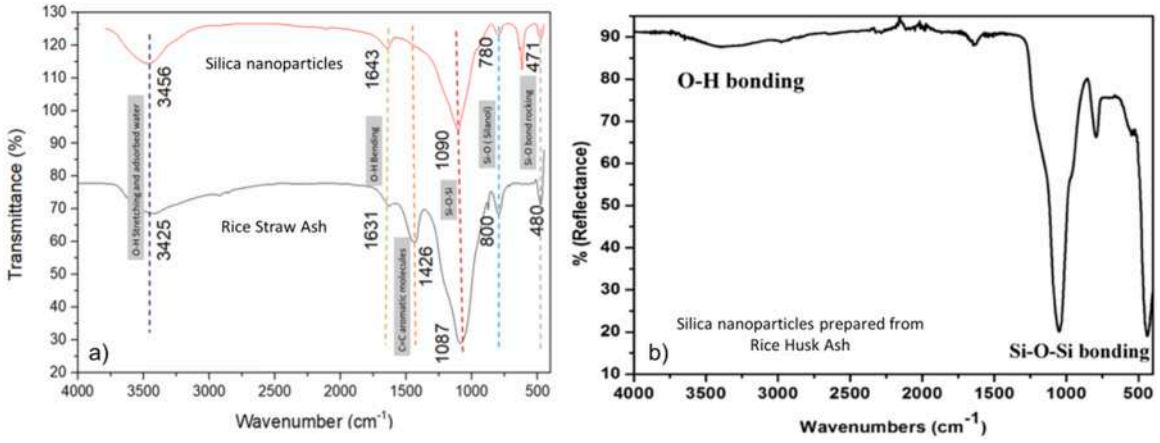

Fig. 10. FTIR spectra of silica material extracted from (a) rice straw ash [170] (b) rice husk ash [9].
(a) Reprinted with permission from Taylor & Francis Online and (b) Reprinted with permission from Elsevier.

Table 9
Typical functional groups observed in MSNs.

Wavenumbers (cm^{-1})	Functional groups
460	Bending vibration of -Si-O-Si-
800	Symmetrical stretching vibration of ≡Si on ≡Si-O-Si≡
970	Stretching vibration Si-O from Si-OH (silanols)
1100	Asymmetric stretching vibration of ≡Si on ≡Si-O-Si≡
1640	Bending vibration of -OH from water molecules
3460	Stretching vibration of -OH from Si-OH (silanol)
1460	C-H bending
2850	C-H symmetric stretching hydrocarbon
2920	C-H asymmetric stretching hydrocarbon

during thermal decomposition. During the first stage (0–120 °C), moderate weight loss was observed possibly due to the existence of H_2O adsorbed on the surface of OH groups of the silica. A slightly higher weight loss was then observed at the second stage (120–330 °C) which can be explained by the decrease of silanol groups. Finally, a sudden drop was observed at the last stage (330 °C) due to the carbonization of volatile materials into gaseous components which occurred at higher temperature. Besides, Miricioiu et al. [107] synthesized MCM-41 from coal FA and their TGA curve of the material was quite different from normal silica nanoparticles where only two intervals of weight losses were observed (Fig. 11 **(b)**). The first stage was due to the loss of water from the silica surface followed by the second stage where the mesoporous structure was disrupted completely. This indicates that the MCM-41 has a low thermal stability as compared to silica produced by Kauldhar and Yadav [164] which is possibly due to the different wall thickness of material and the silica precursor used during the synthesis and the extent of silica condensation within the inorganic pore wall [171].

5. Application of MSNs extracted from waste

Many works have been carried out in producing MSNs from waste and these MSNs have been used in various applications such as adsorbent [172], catalyst [173], drug delivery [174], coating and additives in membrane preparation [175]. Huang et al. [165] synthesized mesoporous silica from boron waste and utilized it as adsorbent for methylene blue removal. The adsorption capacity of MCM-41 produced was 351.7 mg/g at 30 °C and the performances remained constant after 4 times of regeneration. This proposed approach could offer efficient way to recycle waste and at the same time produce cheap silica precursor for MCM-41 synthesis in comparison to commercial MCM-41. Usgodaarachchi et al. [74] also synthesized MSNs from rice husk for the removal of methylene blue from aqueous solution. The MSNs exhibited excellent monolayer capacity of 19.26 mg/g at 298 K which was a favourable nature for the adsorption of methylene blue to the MSN. About 95% of methylene blue removal was achieved in the first 30 min. On the other hand, Wang et al. [176] prepared mesoporous silica nanospheres from

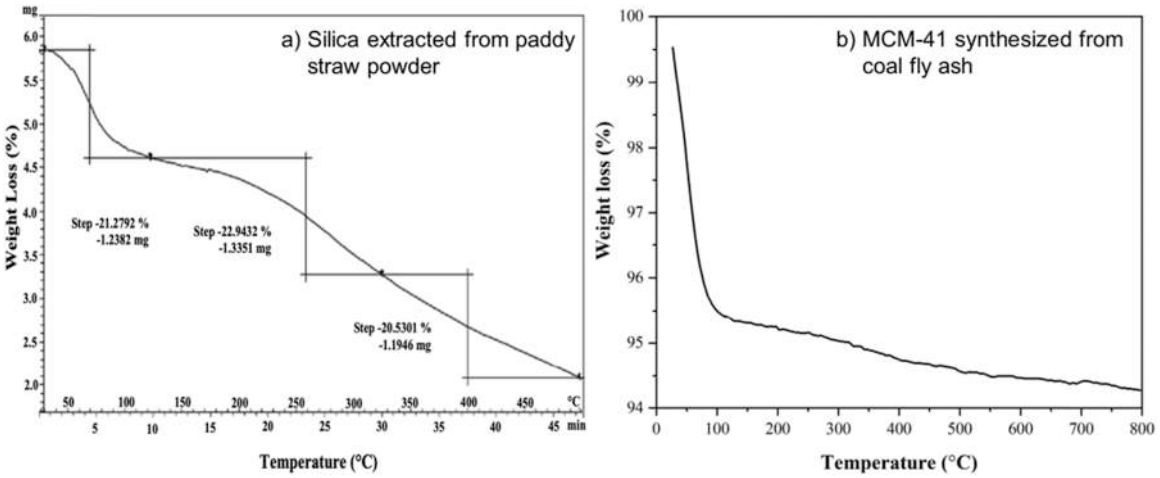

Fig. 11. TGA curves of silica material from (a) paddy straw powder [164] and (b) coal fly ash [107].
(a) Reprinted with permission from Elsevier and (b) Reproduced from MDPI.

coal FA for the uranium U(VI) decontamination. The mesoporous silica displayed high U(VI) removal capacity of 98.9% at the dosage of 600 mg/L due to the interaction between the mesoporous silica and uranyl ions and the oxygen/nitrogen atoms in the amidoxime group. All the studies indicates that the use of MSNs as an adsorbent for the treatment of wastewater are not only effective, but it is also low-cost.

MSNs have also been applied in the fabrication of composite membrane for water and gas separation. Hubadillah et al. [177] used silica extracted from waste rice husk to fabricate ceramic hollow fibre membrane for water filtration application. Highly symmetrical and porous ceramic hollow fibre membrane with a mechanical strength of 71.21 MPa and pure water flux of 303 L/m^2.h was obtained. The low cost and green ceramic hollow fibre membrane also showed a great potential for massive seawater desalination through membrane distillation. This can be an alternative to the commercial of MSNs that is typically much more expensive. In addition, the MSNs can also be used as additive to tailor the membrane properties. Heng et al. incorporated carbon dots grafted silica which was extracted from rice husk into polysulfone (PSf) membrane for dye removal. The membrane had an excellent pure water permeability increment of 111% due to the improved membrane hydrophilicity and enlargement of membrane pores. It also exhibited 50.54% higher dye removal rate compared to pristine PSf membrane. This proves that the application of waste-based MSNs is an economical approach that is useful as an additive for the membrane technology.

MSNs have also been used as adsorbent for gas separation. Park et al. [157] synthesized mesoporous silica using power plant bottom ash powder and used it as a support material for polyethyleneimine (PEI) to capture CO_2. An excellent CO_2 capture capacity of 218 mg/g was successfully achieved. Henao et al.[178] used amine-functionalized mesoporous silica derived from rice husk ash as to capture CO_2. The adsorbent exhibited high CO_2 adsorption capacity of 61.6 mg/g at 40 °C. The performance was outstanding which was attributed to its uniform 2D hexagonal arrangement of cylindrical mesopores that decreased the CO_2 mass transfer resistance and enhanced the interaction with the CO_2 stream. This adsorbent is comparable to the commercialised one. Zinc and carbon functionalized MCM-41 (C-Zn/MCM-41) was synthesised from bagasse heavy ash for the adsorption of volatile organic compounds (VOC) [155]. Compared to other adsorbents, C-Zn/MCM-41 has an outstanding capacity in adsorbing formaldehyde, hexane and toluene.

The use of extracted silica as a catalyst support has also been investigated. Silica extracted from sugarcane bagasse ash and pumice stone were used as the catalyst support for silver in the 4-nitrophenol reduction reaction [159]. The Ag_2O/SiO_2 from pumice stone showed a higher reaction rate of 0.0561 min^{-1} compared to the ones prepared using sugarcane bagasse ash due to its smaller particle size. However, further research is still required to improve the properties of extracted silica particularly in terms of reaction rate. Ramalingam et al. [179] used ruthenium/copper nanoparticles incorporated with mesoporous silica derived from rice husk ash for catalytic acetylation of glycerol. The catalyst showed a high conversion of 98% and high shape selectivity towards monoacetin formation of. Therefore, the as-prepared catalyst can be used for a large-scale synthesis of renewable chemical products and in acetylation reaction.

All of these studies indicated that the performances of silica nanoparticles extracted either from agricultural or industrial waste are comparable to the commercial silica. This clearly suggests the potential of using waste as a silica source for the synthesis of silica nanoparticles. Such practice is of great benefit to the future chemical processes towards cleaner production and circular economy.

6. Challenges and future prospective

Many commercial MSNs are produced using high-cost templates and surfactants. In addition, the use of acid washing under high temperature and atmospheric pressure makes the process of MSNs production costly. As a sustainable solution, agricultural and industrial waste could be utilized as precursor for MSNs synthesis. Table 10 shows the estimation cost of MSNs produced from waste and from the current commercial process. The evaluation is based on the price of raw materials and energy used during the production. The value is compared with the price of commercial silica of particle size of 10–20 nm and purity of 99.5%. The

Table 10
Cost estimation of silica production per kg using waste as a source.

	Commercial method	Unit price	Chemical method	Unit price
Precursor type and cost	Sodium meta silicate Tetraethyl orthosilicate	$ 60/kg $142/ 100 mL	Agricultural/ Industrial waste	$ 0
Chemical type and cost	CO_2	$ 115/L	NaOH HCl	$88/kg $90.30/L
Processing temperature	1300 °C	–	80–120 °C	–
Power required	11–13 MW/h[9]	$0.89 per KW	1.5 kW/h [9]	$0.07 per KW
[a]Market price nano silica	$1330/kg			

[a] The price was accessed from Sigma-Aldrich website (https://www.sigmaaldrich.com/).

extraction of silica using conventional commercial process is typically energy and cost intensive due to the use of expensive precursors and high processing temperature. In addition, high amount of CO_2 is released during the synthesis process, which contribute to environmental and global warming issue. Thus, a simple and economic viable approach of waste utilization and waste minimization can produce nano silica comparatively cheaper and less energy intensive than the commercial one.

While the concept of turning waste into advanced technologies for environmental applications may look like an attractive full-circle approach, there are significant knowledge gaps about engineered MSNs that should be addressed before transitioning these ideas from the lab to the real world. One major challenge in the synthesis of MSNs is how to maintain the characteristics and quality consistency of the material. Among methods available for silica nanoparticles synthesis, chemical routes remain popular due to the ease of control and high purity product. However, not many studies have provided insights into the synthesis and growth mechanisms for the formation of different types of silica nanoparticles. To date, there is a lack of general principles to guide the design and synthesis routes of MSNs to meet specific functional requirements. As a result, there is a need for a better understanding and control of the synthesis process to ensure reproducibility in the product. The agglomeration of MSNs is also an inherent issue that substantially damages the performance in relevant fields. Most nanomaterials start to agglomerate due to physical entanglement, electrostatic interactions, or high surface energy during the synthesis conditions. Finding a way to minimize the agglomeration of nanoparticles, particularly during the synthesis process, will also aids the leap from laboratory to commercial applications. It can be concluded that simplicity of synthesis method, environmentally friendly silica precursor and low cost of raw material are the key features of using agricultural and industrial waste to produce sustainable and greener MSNs.

Declaration of Competing Interest

The authors declare that they have no known competing financial interests or personal relationships that could have appeared to influence the work reported in this paper.

Acknowledgement

The authors would like to acknowledge Universiti Teknologi MARA, Malaysia for internal grant funding (600-RMC/MYRA 5/3/LESTARI (052/2020)). N.A.A Razak wishes to express her gratitude to Advanced Membrane Technology Research Centre (AMTEC), Universiti Teknologi Malaysia for granting visiting fellowship (HICOE AMTEC (A. J090301.5300.07092)).

References

[1] L. Chen, J. Liu, Y. Zhang, G. Zhang, Y. Kang, A. Chen, X. Feng, L. Shao, The toxicity of silica nanoparticles to the immune system, Nanomedicine 13 (2018) 1939–1962, https://doi.org/10.2217/nnm-2018-0076.

[2] G.A. Seisenbaeva, L.M.A. Ali, A. Vardanyan, M. Gary-Bobo, T.M. Budnyak, V. G. Kessler, J.O. Durand, Mesoporous silica adsorbents modified with amino polycarboxylate ligands – functional characteristics, health and environmental effects, J. Hazard. Mater. 406 (2021), 124698, https://doi.org/10.1016/j.jhazmat.2020.124698.

[3] F.N. Buyuknalcaci, Y. Polat, T.A. Negawo, E. Döner, M.S. Alam, T. Hamouda, A. Kilic, Carbon nanotube-based nanocomposites for wind turbine applications, in: Polymer-based Nanocomposites for Energy and Environmental Applications, Woodhead Publishing, 2018, pp. 635–661, https://doi.org/10.1016/B978-0-08-102262-7.00024-6.

[4] R. Narayan, U.Y. Nayak, A.M. Raichur, S. Garg, Mesoporous silica nanoparticles: a comprehensive review on synthesis and recent advances, Pharmaceutics 10 (2018) 1–49, https://doi.org/10.3390/pharmaceutics10030118.

[5] P.N.E. Diagboya, E.D. Dikio, Silica-based mesoporous materials; emerging designer adsorbents for aqueous pollutants removal and water treatment, Microporous Mesoporous Mater. 266 (2018) 252–267, https://doi.org/10.1016/j.micromeso.2018.03.008.

[6] M.Y. Nassar, I.S. Ahmed, M.A. Raya, A facile and tunable approach for synthesis of pure silica nanostructures from rice husk for the removal of ciprofloxacin drug from polluted aqueous solutions, J. Mol. Liq. 282 (2019) 251–263, https://doi.org/10.1016/j.molliq.2019.03.017.

[7] G. Guzel Kaya, E. Yilmaz, H. Deveci, Synthesis of sustainable silica xerogels/aerogels using inexpensive steel slag and bean pod ash: a comparison study, Adv. Powder Technol. 31 (2020) 926–936, https://doi.org/10.1016/j.apt.2019.12.013.

[8] P.S. Shinde, P.S. Suryawanshi, K.K. Patil, V.M. Belekar, S.A. Sankpal, S. D. Delekar, S.A. Jadhav, A brief overview of recent progress in porous silica as catalyst supports, J. Compos. Sci. 5 (2021) 1–17, https://doi.org/10.3390/jcs5030075.

[9] S. Mor, C.K. Manchanda, S.K. Kansal, K. Ravindra, Nanosilica extraction from processed agricultural residue using green technology, J. Clean. Prod. 143 (2017) 1284–1290, https://doi.org/10.1016/j.jclepro.2016.11.142.

[10] V. Zarei, M. Mirzaasadi, A. Davarpanah, A. Nasiri, M. Valizadeh, M.J.S. Hosseini, Environmental method for synthesizing amorphous silica oxide nanoparticles from a natural material, Processes 9 (2021) 1–9, https://doi.org/10.3390/pr9020334.

[11] P.E. Imoisili, K.O. Ukoba, T.C. Jen, Synthesis and characterization of amorphous mesoporous silica from palm kernel shell ash, Bol. La Soc. Esp. Ceram. Y. Vidr. 59 (2020) 159–164, https://doi.org/10.1016/j.bsecv.2019.09.006.

[12] V.K. Yadav, M.H. Fulekar, Green synthesis and characterization of amorphous silica nanoparticles from fly ash, Mater. Today Proc. 18 (2019) 4351–4359, https://doi.org/10.1016/j.matpr.2019.07.395.

[13] S. Saini, A. Gupta, A.J. Mehta, S. Pramanik, Rice husk-extracted silica reinforced graphite/aluminium matrix hybrid composite, Sci. Rep. 10 (2020), 20219, https://doi.org/10.1007/s10973-020-10404-8.

[14] F. Farirai, M. Mupa, M.O. Daramola, An improved method for the production of high purity silica from sugarcane bagasse ash obtained from a bioethanol plant boiler, Part. Sci. Technol. (2020), https://doi.org/10.1080/02726351.2020.1734700.

[15] P.E. Imoisili, K.O. Ukoba, T.C. Jen, Green technology extraction and characterisation of silica nanoparticles from palm kernel shell ash via sol-gel, J. Mater. Res. Technol. 9 (2020) 307–313, https://doi.org/10.1016/j.jmrt.2019.10.059.

[16] S. Dey, D. Ray, A. Mondal, T.K. Parya, Effect of yttria on sintering and microstructural behavior of reaction sintered mullite based on bauxite, fly ash and precipitated silica, Ceram. Int. 44 (2018) 10087–10093, https://doi.org/10.1016/j.ceramint.2018.02.214.

[17] Z. Zhou, M. Sofi, J. Liu, S. Li, A. Zhong, P. Mendis, Nano-CSH modified high volume fly ash concrete: early-age properties and environmental impact analysis, J. Clean. Prod. 286 (2021), 124924, https://doi.org/10.1016/j.jclepro.2020.124924.

[18] K. Zulkifly, H. Cheng-Yong, L. Yun-Ming, M.M.A.B. Abdullah, O. Shee-Ween, M.S. Bin Khalid, Effect of phosphate addition on room-temperature-cured fly ash-metakaolin blend geopolymers, Constr. Build. Mater. 270 (2021), 121486, https://doi.org/10.1016/j.conbuildmat.2020.121486.

[19] K. Dlomo, S.M. Mohomane, T.E. Motaung, Influence of silica nanoparticles on the properties of cellulose composite membranes: a current review, Cellul. Chem. Technol. 54 (2020) 765–775, https://doi.org/10.35812/CelluloseChemTechnol.2020.54.76.

[20] E. Reverchon, R. Adami, Nanomaterials and supercritical fluids, J. Supercrit. Fluids 37 (2006) 1–22, https://doi.org/10.1016/j.supflu.2005.08.003.

[21] H.Y. Lian, Z.K. Kao, Y.C. Liao, Y. Yamauchi, K.C.W. Wu, Self-assembled mesoporous silica nanoparticles in controlled patterns produced by soft-lithography and ink-jet printing, J. Nanosci. Nanotechnol. 13 (2013) 2804–2808, https://doi.org/10.1166/jnn.2013.7339.

[22] S.D. Doke, C.M. Patel, V.N. Lad, Improving performance of the synthesis of silica nanoparticles by surfactant-incorporated wet attrition milling, Silicon (2021), https://doi.org/10.1007/s12633-020-00871-x.

[23] S. Sankar, N. Kaur, S. Lee, D.Y. Kim, Rapid sonochemical synthesis of spherical silica nanoparticles derived from brown rice husk, Ceram. Int. 44 (2018) 8720–8724, https://doi.org/10.1016/j.ceramint.2018.02.090.

[24] W.K. Setiawan, N.S. Indrasti, Suprihatin, Synthesis and characterization of nanosilica from boiler ash with co-precipitation method, in: 3rd Int. Conf. Adapt. Intell. Agroindustry (3rd ICAIA), 2015: pp. 160–164.

[25] I. Made Joni, Rukiah, C. Panatarani, Synthesis of silica particles by precipitation method of sodium silicate: effect of temperature, pH and mixing technique, AIP Conf. Proc. 2219 (2020), 080018, https://doi.org/10.1063/5.0003074.

[26] I.A. Rahman, V. Padavettan, Synthesis of Silica nanoparticles by Sol-Gel: size-dependent properties, surface modification, and applications in silica-polymer nanocompositesa review, J. Nanomater. 2012 (2012) 1–15, https://doi.org/10.1155/2012/132424.

[27] G. Priyadarshana, N. Kottegoda, A. Senaratne, A. De Alwis, V. Karunaratne, Synthesis of magnetite nanoparticles by top-down approach from a high purity ore, J. Nanomater. 2015 (2015) 1–8, https://doi.org/10.1155/2015/317312.

[28] H. Barabadi, T.J. Webster, H. Vahidi, H. Sabori, K. Damavandi Kamali, F. Jazayeri Shoushtari, M.A. Mahjoub, M. Rashedi, E. Mostafavi, D. Medina Cruz, O. Hosseini, M. Saravana, Green nanotechnology-based gold nanomaterials for hepatic cancer therapeutics: a systematic review, Iran. J. Pharm. Res 19 (2020) 3–17, https://doi.org/10.22037/ijpr.2020.113820.14504.

[29] A. Agrawal , G.-C. Yi , Chapter two - Sample pretreatment with graphene materials C.M.B.T.-C.A.C. Hussain Anal. Appl. Graphene Compr. Anal. Chem. 2020 Elsevier 21 47 doi: 10.1016/bs.coac.2020.08.012.

[30] M. Salavati-Niasari, J. Javidi, M. Dadkhah, Ball milling synthesis of silica nanoparticle from rice husk ash for drug delivery application, Comb. Chem. High. Throughput Screen. 16 (2013) 458–462, https://doi.org/10.2174/1386207311316060006.

[31] D. Srinivasa, B. Blumenauer, M.W. Clemens, Chapter 4 - Surgical implications of surface texturing in breast implants**No author has any financial interests in relation to the context of this article, in: C. Mathur (Ed.), Nanotechnology in Cancer, William Andrew Publishing, 2017, pp. 71–85, https://doi.org/10.1016/B978-0-323-39080-4.00004-5 (A.B.B.T.-N. in).

[32] R. Jose Varghese, E.H.M. Sakho, S. Parani, S. Thomas, O.S. Oluwafemi, J. Wu, Chapter 3 - Introduction to Nanomaterials: Synthesis and Applications, in: S. Thomas, E.H.M. Sakho, N. Kalarikkal, S.O. Oluwafemi, J.B.T.-N. for S.C.A. Wu (Eds.), Elsevier, 2019, pp. 75–95, https://doi.org/10.1016/B978-0-12-813337-8.00003-5.

[33] T.J. Merkel, K.P. Herlihy, J. Nunes, R.M. Orgel, J.P. Rolland, J.M. DeSimone, Scalable, shape-specific, top-down fabrication methods for the synthesis of engineered colloidal particles, Langmuir 26 (2010) 13086–13096, https://doi.org/10.1021/la903890h.

[34] E.M. Modan, A.G. Plaiasu, Advantages and disadvantages of chemical methods in the elaboration of nanomaterials, Ann. "Dunarea Jos" Univ. Galati. Fascicle IX, Metall. Mater. Sci. 43 (2020) 53–60, https://doi.org/10.35219/mms.2020.1.08.

[35] S.A.M. Zobir, S.A. Rashid, T. Tan, Recent development on the synthesis techniques and properties of graphene derivatives, Synth. Technol. Appl. Carbon Nanomater (2018), https://doi.org/10.1016/B978-0-12-815757-2.00004-8.

[36] M.B. Tahir, M. Rafique, M.S. Rafique, T. Nawaz, M. Rizwan, M. Tanveer, Photocatalytic nanomaterials for degradation of organic pollutants and heavy metals, in: Nanotechnology and Photocatalysis for Environmental Applications, Elsevier Inc, 2020, pp. 119–138, https://doi.org/10.1016/C2019-0-00295-6.

[37] K.V. Madhuri, Thermal protection coatings of metal oxide powders, in: Y. Al-Douri (Ed.), Metal Oxide Powder Technologies, Elsevier Inc, 2020, pp. 209–231, https://doi.org/10.1016/C2018-0-02252-5.

[38] Z. Huang, Y. Huang, L. Zheng, G. Zhang, Effects of precursors on silica particle generation in CVD synthesis for fused silica glass, J. Non Cryst. Solids 499 (2018) 86–94, https://doi.org/10.1016/j.jnoncrysol.2018.07.020.

[39] S.D. Karande, S.A. Jadhav, H.B. Garud, V.A. Kalantre, S.H. Burungale, P.S. Patil, Green and sustainable synthesis of silica nanoparticles, Nanotechnol. Environ. Eng. 6 (2021) 29, https://doi.org/10.1007/s41204-021-00124-1.

[40] N. Silmi, E. Febriyanti, A. Andriani, R. Arsyad, F.V. Steky, R.R. Mukti, V. Suendo, Textural control of bicontinuous concentric lamellar nanostructured mesoporous silica via low-pressure solvothermal method, Mater. Chem. Phys. 265 (2021), 124492, https://doi.org/10.1016/j.matchemphys.2021.124492.

[41] P.S. Utama, E. Saputra, Khairat, Effective utilizations of palm oil mill fly ash for synthetic amorphous silica and carbon zeolite composite synthesis, IOP Conf. Ser. Mater. Sci. Eng. 345 (2018), 012009, https://doi.org/10.1088/1757-899X/345/1/012009.

[42] M. Sajid, J. Płotka-Wasylka, Nanoparticles: synthesis, characteristics, and applications in analytical and other sciences, Microchem. J. 154 (2020), 104623, https://doi.org/10.1016/j.microc.2020.104623.

[43] F.R.D. Fernandes, F.G.H.S. Pinto, E.L.F. Lima, L.D. Souza, V.P.S. Caldeira, A.G. D. Santos, Influence of synthesis parameters in obtaining KIT-6 mesoporous material, Appl. Sci. 8 (2018) 725, https://doi.org/10.3390/app8050725.

[44] A. Cid, Synthesis of NPs by Microemulsion Method, Micro A Chem. Nanoreactor (2018) 1–15, https://doi.org/10.5772/intechopen.80633.

[45] M. Kamali, R. Dewil, L. Appels, T.M. Aminabhavi, Nanostructured materials via green sonochemical routes – sustainability aspects, Chemosphere 276 (2021), 130146, https://doi.org/10.1016/j.chemosphere.2021.130146.

[46] Z. Li, T. Zhuang, J. Dong, L. Wang, J. Xia, H. Wang, X. Cui, Z. Wang, Sonochemical fabrication of inorganic nanoparticles for applications in catalysis, Ultrason. Sonochem. 71 (2021), 105384, https://doi.org/10.1016/j.ultsonch.2020.105384.

[47] K. Babooram, 28 - Novel solution routes to ferroelectrics and relaxors, in: Handbook of Advanced Dielectric, Piezoelectric and Ferroelectric Materials, Woodhead Publishing, 2008, pp. 852–883, https://doi.org/10.1533/9781845694005.7.852 (Z.-G.B.T.-H. of A.D. Ye Piezoelectric and Ferroelectric Materials).

[48] A.V. Rane, K. Kanny, V.K. Abitha, S. Thomas, Chapter 5 - methods for synthesis of nanoparticles and fabrication of nanocomposites, in: S. Mohan Bhagyaraj, O. S. Oluwafemi, N. Kalarikkal, S.B.T.-S. of I.N. Thomas (Eds.), Synthesis of Inorganic Nanomaterials, Woodhead Publishing, 2018, pp. 121–139, https://doi.org/10.1016/B978-0-08-101975-7.00005-1.

[49] S. Liu, C. Ma, M.-G. Ma, F. Xu, 12 - Magnetic Nanocomposite Adsorbents, in: G. Z. Kyzas, A.C.B.T.-C.N. Mitropoulos (Eds.), Composite Nanoadsorbents, Elsevier, 2019, pp. 295–316, https://doi.org/10.1016/B978-0-12-814132-8.00013-7.

[50] W. Stöber, A. Fink, E. Bohn, Controlled growth of monodisperse silica spheres in the micron size range, J. Colloid Interface Sci. 26 (1968) 62–69, https://doi.org/10.1016/0021-9797(68)90272-5.

[51] S. Dervin, S.C. Pillai, An Introduction to Sol-Gel Processing for Aerogels, in: S. C. Pillai, S. Hehir (Eds.), Springer International Publishing, Cham, 2017, pp. 1–22, https://doi.org/10.1007/978-3-319-50144-4_1.

[52] W.H. Kwan, Y.S. Wong, Acid leached rice husk ash (ARHA) in concrete: a review, Mater. Sci. Energy Technol. 3 (2020) 501–507, https://doi.org/10.1016/j.mset.2020.05.001.

[53] S. Azat, Z. Sartova, K. Bekseitova, K. Askaruly, Extraction of high-purity silica from rice husk via hydrochloric acid leaching treatment, Turk. J. Chem. 43 (2019) 1258–1269, https://doi.org/10.3906/kim-1903-53.

[54] N.H. Do, H.H. Pham, T.M. Le, J. Lauwaert, L. Diels, A. Verberckmoes, N.H.N. Do, V.T. Tran, P.K. Le, The novel method to reduce the silica content in lignin recovered from black liquor originating from rice straw, Sci. Rep. 10 (2020) 21263, https://doi.org/10.1038/s41598-020-77867-5.

[55] M.F. Anuar, Y.W. Fen, M.H.M. Zaid, K.A. Matori, R.E.M. Khaidir, Synthesis and structural properties of coconut husk as potential silica source, Results Phys. 11 (2018) 1–4, https://doi.org/10.1016/j.rinp.2018.08.018.

[56] J. Chun, J.H. Lee, Recent progress on the development of engineered silica particles derived from rice husk, Sustain. (2020). ⟨https://doi.org/10.3390/su122410683⟩.

[57] L. Rodriguez-Freire, J. Gonzalez-Estrella, G. Li, Chapter 15 - Technologies for fractionation of wastewater and resource recovery, in: J.A. Olivares, D. Puyol, J. A. Melero (Eds.), Elsevier, 2020, pp. 329–354, https://doi.org/10.1016/B978-0-12-816204-0.00015-1.

[58] H. Elomaa, S. Seisko, J. Lehtola, M. Lundström, A study on selective leaching of heavy metals vs. iron from fly ash, J. Mater. Cycles Waste Manag. 21 (2019) 1004–1013, https://doi.org/10.1007/s10163-019-00858-w.

[59] D. Das, S. Mukherjee, M.G. Chaudhuri, Studies on leaching characteristics of electronic waste for metal recovery using inorganic and organic acids and base, Waste Manag. Res. 39 (2020) 242–249, https://doi.org/10.1177/0734242×20931929.

[60] D. Valeev, A. Mikhailova, A. Atmadzhidi, Kinetics of iron extraction from coal fly ash by hydrochloric acid leaching, Metals 8 (2018) 533, https://doi.org/10.3390/met8070533.

[61] N.N. Maseko, D. Schneider, S. Wassersleben, D. Enke, S.A. Iwarere, J. Pocock, A. Stark, The production of biogenic silica from different south african agricultural residues through a thermo-chemical treatment method, Sustain 13 (2021) 1–14, https://doi.org/10.3390/su13020577.

[62] M. Gao, Q. Ma, Q. Lin, J. Chang, H. Ma, A novel approach to extract SiO2 from fly ash and its considerable adsorption properties, Mater. Des. 116 (2017) 666–675, https://doi.org/10.1016/j.matdes.2016.12.028.

[63] J. Wang, L. Fang, F. Cheng, X. Duan, R. Chen, Hydrothermal synthesis of SBA-15 using sodium silicate derived from coal gangue, J. Nanomater 2013 (2013) 1–7, https://doi.org/10.1155/2013/352157.

[64] M.F. Hamza, J.-C. Roux, E. Guibal, Metal valorization from the waste produced in the manufacturing of Co/Mo catalysts: leaching and selective precipitation, J. Mater. Cycles Waste Manag. 21 (2019) 525–538, https://doi.org/10.1007/s10163-018-0811-9.

[65] W. Xu, J. Wei, J. Chen, B. Zhang, P. Xu, J. Ren, Q. Yu, Comparative study of water-leaching and acid-leaching pretreatment on the thermal stability and reactivity of biomass silica for viability as a pozzolanic additive in cement, Materials 11 (2018) 1697, https://doi.org/10.3390/ma11091697.

[66] S. Azat, A.V. Korobeinyk, K. Moustakas, V.J. Inglezakis, Sustainable production of pure silica from rice husk waste in Kazakhstan, J. Clean. Prod. 217 (2019) 352–359, https://doi.org/10.1016/j.jclepro.2019.01.142.

[67] R.K. Taggart, J.C. Hower, H. Hsu-Kim, Effects of roasting additives and leaching parameters on the extraction of rare earth elements from coal fly ash, Int. J. Coal Geol. 196 (2018) 106–114, https://doi.org/10.1016/j.coal.2018.06.021.

[68] J.T. Librea, F.D. Dacanay, Z.Z. Martin, L.L. Diaz, Effect of water and acid pre-treatment on the physicochemical properties of rice husk for silica extraction, IOP Conf. Ser. Mater. Sci. Eng. 540 (2019), 012007, https://doi.org/10.1088/1757-899x/540/1/012007.

[69] P. Chindaprasirt, U. Rattanasak, Eco-production of silica from sugarcane bagasse ash for use as a photochromic pigment filler, Sci. Rep. 10 (2020) 9890, https://doi.org/10.1038/s41598-020-66885-y.

[70] S. Steven, E. Restiawaty, P. Pasymi, Y. Bindar, An appropriate acid leaching sequence in rice husk ash extraction to enhance the produced green silica quality for sustainable industrial silica gel purpose, J. Taiwan Inst. Chem. Eng. 122 (2021) 51–57, https://doi.org/10.1016/j.jtice.2021.04.053.

[71] Y. Lu, A. Tian, J. Zhang, Y. Tang, P. Shi, Q. Tang, Y. Huang, Physical and chemical properties, pretreatment, and recycling of municipal solid waste incineration fly ash and bottom ash for highway engineering: a literature review, J. Comput. Biol. 2020 (2020), 8886134, https://doi.org/10.1155/2020/8886134.

[72] Y. Zhao, Y. Zheng, H. He, Z. Sun, A. Li, Silica extraction from bauxite reaction residue and synthesis water glass, Green. Process. Synth. 10 (2021) 268–283, https://doi.org/10.1515/gps-2021-0028.

[73] N.S. Osman, N. Sapawe, Preparation of amorphous oil palm frond ash (OPFA) via acid leaching treatment as precursor for silica synthesis, Mater. Today Proc. 31 (2020) 253–256, https://doi.org/10.1016/j.matpr.2020.05.333.

[74] L. Usgodaarachchi, C. Thambiliyagodage, R. Wijesekera, M.G. Bakker, Synthesis of mesoporous silica nanoparticles derived from rice husk and surface-controlled amine functionalization for efficient adsorption of methylene blue from aqueous solution, Curr. Res. Green. Sustain. Chem. 4 (2021), 100116, https://doi.org/10.1016/j.crgsc.2021.100116.

[75] S. Gao, Y. Zhang, Y. Zhang, S. Sun, M. Wang, Study on the extracted process of mullite from coal fly ash by-product sodium silicate, J. Ceram. Soc. Jpn. 127 (2019) 90–97, https://doi.org/10.2109/jcersj2.18067.

[76] N.F. Bain, C.Z.A. Abidin, W.N. Kamaruzaman, N.S. Arbaan, Bottom ash treatment by using seawater with Citrus aurantifolia, IOP Conf. Ser. Earth Environ. Sci. 646 (2021), 012009, https://doi.org/10.1088/1755-1315/646/1/012009.

[77] M. Faris, Production of silica from mustard husk ash, Mod. Approaches Mater. Sci. 4 (2021) 525–529, https://doi.org/10.32474/MAMS.2021.04.000188.

[78] V.H. Le, C.N.H. Thuc, H.H. Thuc, Synthesis of silica nanoparticles from Vietnamese rice husk by sol–gel method, Nanoscale Res. Lett. 8 (2013) 58, https://doi.org/10.1186/1556-276x-8-58.

[79] F. Fajaroh, S. Nazriati, Effect of concentration of sodium silicate solution in the synthesis of silica-coated magnetite nanoparticles by ultrasonication, AIP Conf. Proc. 1710 (2016), 030018, https://doi.org/10.1063/1.4941484.

[80] N.K. Sethy, Z. Arif, P.K. Mishra, P. Kumar, Synthesis of SiO2 nanoparticle from bamboo leaf and its incorporation in PDMS membrane to enhance its separation properties, J. Polym. Eng. 39 (2019) 679–687, https://doi.org/10.1515/polyeng-2019-0120.

[81] I. Fatimah, G. Fadillah, I. Sahroni, A. Kamari, S. Sagadevan, R.A. Doong, Nanoflower-like composites of ZnO/SiO2 synthesized using bamboo leaves ash as reusable photocatalyst, Arab. J. Chem. 14 (2021), 102973, https://doi.org/10.1016/j.arabjc.2020.102973.

[82] A. Jumari, C.S. Yudha, H. Widiyandari, A.P. Lestari, SiO2/C composite as a high capacity anode materials of LiNi0.8Co0.15Al0.05O2 battery derived from coal combustion fly ash, Appl. Sci. 10 (2020) 8428.

[83] J.Y. Park, Y.M. Gu, S.Y. Park, E.T. Hwang, B.I. Sang, J. Chun, J.H. Lee, Two-stage continuous process for the extraction of silica from rice husk using attrition ball milling and alkaline leaching methods, Sustain 13 (2021), https://doi.org/10.3390/su13137350.

[84] T.T. Nguyen, H.T. Ma, P. Avti, M.J.K. Bashir, C.A. Ng, L.Y. Wong, H.K. Jun, Q. M. Ngo, N.Q. Tran, Adsorptive removal of iron using SiO(2) nanoparticles extracted from rice husk ash, J. Anal. Methods Chem. 2019 (2019), 6210240, https://doi.org/10.1155/2019/6210240.

[85] J.F.F. Donanta Dhaneswara Frans Wensten Situmorang, A.N. Haqoh, Synthesis of amorphous silica from rice husk ash: comparing HCl and CH3COOH acidification methods and various alkaline concentrations, Int. J. Technol. 11 (2020) 291–319.

[86] P.P. Nayak, S. Nandi, A.K. Datta, Comparative assessment of chemical treatments on extraction potential of commercial grade silica from rice husk, Eng. Rep. 1 (2019), e12035, https://doi.org/10.1002/eng2.12035.

[87] Q. Alam, Y. Hendrix, L. Thijs, A. Lazaro, K. Schollbach, H.J.H. Brouwers, Novel low temperature synthesis of sodium silicate and ordered mesoporous silica from incineration bottom ash, J. Clean. Prod. 211 (2019) 874–883, https://doi.org/10.1016/j.jclepro.2018.11.173.

[88] I. Haq, K. Akhtar, A. Malik, Effect of experimental variables on the extraction of silica from the rice husk ash, J. Chem. Soc. Pak. 36 (2014) 382–387.

[89] N. Surayah Osman, N. Sapawe, High purity and amorphous silica (SiO2) prepared from oil palm frond (OPF) through sol–gel method, Mater. Today Proc. 31 (2020) 228–231, https://doi.org/10.1016/j.matpr.2020.05.299.

[90] N. Nazriati, H. Setyawan, S. Affandi, M. Yuwana, S. Winardi, Using bagasse ash as a silica source when preparing silica aerogels via ambient pressure drying, J. Non Cryst. Solids 400 (2014) 6–11, https://doi.org/10.1016/j.jnoncrysol.2014.04.027.

[91] A.D. Li, W.C. Liu, 4 - Optical properties of ferroelectric nanocrystal/polymer composites, in: S.C. Tjong, P.N. Mai (Eds.), Physical Properties and Applications of Polymer Nanocomposites, Woodhead Publishing, 2010, pp. 108–158, https://doi.org/10.1533/9780857090249.1.108.

[92] E. Suvaci, E. Özel, Hydrothermal Synthesis, in: G. Pomeroy (Ed.), Elsevier, Oxford, 2021, pp. 59–68, https://doi.org/10.1016/B978-0-12-803581-8.12096-X.

[93] Y.X. Gan, A.H. Jayatissa, Z. Yu, X. Chen, M. Li, Hydrothermal synthesis of nanomaterials, J. Comput. Biol. J. Comput. Mol. Cell Biol. 2020 (2020), https://doi.org/10.1155/2020/8917013.

[94] G. Yang, S.-J. Park, Conventional and microwave hydrothermal synthesis and application of functional materials: a review, Materials 12 (2019) 3640, https://doi.org/10.3390/ma12071177.

[95] B. Wang, Y. Zhou, L. Li, H. Xu, Y. Sun, Y. Wang, Novel synthesis of cyano-functionalized mesoporous silica nanospheres (MSN) from coal fly ash for removal of toxic metals from wastewater, J. Hazard. Mater. 345 (2018) 76–86, https://doi.org/10.1016/j.jhazmat.2017.10.063.

[96] A. Arumugam, G. Karuppasamy, G.B. Jegadeesan, Synthesis of mesoporous materials from bamboo leaf ash and catalytic properties of immobilized lipase for hydrolysis of rubber seed oil, Mater. Lett. 225 (2018) 113–116, https://doi.org/10.1016/j.matlet.2018.04.122.

[97] A. Bathla, C. Narula, R.P. Chauhan, Hydrothermal synthesis and characterization of silica nanowires using rice husk ash: an agricultural waste, J. Mater. Sci. Mater. Electron. 29 (2018) 6225–6231, https://doi.org/10.1007/s10854-018-8598-y.

[98] H. Meléndez-Ortiz, A. Mercado-Silva, L. García-Cerda, G. Castruita, Y. Perera-Mercado, Hydrothermal synthesis of mesoporous silica MCM-41 using commercial sodium silicate, J. Mex. Chem. Soc. 57 (2013) 73–79, https://doi.org/10.29356/jmcs.v57i2.215.

[99] T.H. Liou, Y.K. Tseng, S.M. Liu, Y.T. Lin, S.Y. Wang, R.T. Liu, Green synthesis of mesoporous graphene oxide/silica nanocomposites from rich husk ash: Characterization and adsorption performance, Environ. Technol. Innov. 22 (2021), 101424, https://doi.org/10.1016/j.eti.2021.101424.

[100] I. Fatimah, S.N. Amaliah, M.F. Andrian, T.P. Handayani, R. Nurillahi, N. I. Prakoso, W.P. Wicaksono, L. Chuenchom, Iron oxide nanoparticles supported on biogenic silica derived from bamboo leaf ash for rhodamine B photodegradation, Sustain. Chem. Pharm. 13 (2019), 100149, https://doi.org/10.1016/j.scp.2019.100149.

[101] R. Sun, P. Qiao, Z. Wang, W. Wang, Monodispersed large-mesopore mesoporous silica nanoparticles enabled by sulfuric acid assisted hydrothermal process, Microporous Mesoporous Mater. 317 (2021), 111023. ⟨https://doi.org/10.1016/j.micromeso.2021.111023⟩.

[102] K. Bai, J. Hao, Y. Yang, A. Qian, The effect of hydrothermal temperature on the properties of SBA-15 materials, Heliyon 6 (2020), e04436, https://doi.org/10.1016/j.heliyon.2020.e04436.

[103] N. Juárez-Serrano, D. Berenguer, I. Martínez-Castellanos, I. Blasco, M. Beltrán, A. Marcilla, Effect of reaction time and hydrothermal treatment time on the textural properties of SBA-15 synthesized using sodium silicate as a silica source and its efficiency for reducing tobacco smoke toxicity, Catal 11 (2021), https://doi.org/10.3390/catal11070808.

[104] I. Majchrzak-Kucęba, W. Nowak, Characterization of MCM-41 mesoporous materials derived from polish fly ashes, Int. J. Miner. Process. 101 (2011) 100–111, https://doi.org/10.1016/j.minpro.2011.09.002.

[105] G.M.K. Tolba, N.A.M. Barakat, A.M. Bastaweesy, E.A. Ashour, W. Abdelmoez, M. H. El-Newehy, S.S. Al-Deyab, H.Y. Kim, Effective and highly recyclable nanosilica produced from the rice husk for effective removal of organic dyes, J. Ind. Eng. Chem. 29 (2015) 134–145, https://doi.org/10.1016/j.jiec.2015.03.025.

[106] M.U. Cornelius, Synthesis and characterisation of high silica zeolites with MOR and MFI framework type from South African coal fly ash, University of the Western Cape, 2019.

[107] M.G. Miricioiu, V.C. Niculescu, C. Filote, M.S. Raboaca, G. Nechifor, Coal fly ash derived silica nanomaterial for mmms-application in CO_2/CH4 separation, Membranes 11 (2021) 1–18, https://doi.org/10.3390/membranes11020078.

[108] K. Bunmai, N. Osakoo, K. Deekamwong, W. Rongchapo, C. Keawkumay, N. Chanlek, S. Prayoonpokarach, J. Wittayakun, Extraction of silica from cogon grass and utilization for synthesis of zeolite NaY by conventional and microwave-assisted hydrothermal methods, J. Taiwan Inst. Chem. Eng. 83 (2018) 152–158, https://doi.org/10.1016/j.jtice.2017.11.024.

[109] G. Lawrence, A.V. Baskar, M.H. El-Newehy, W.S. Cha, S.S. Al-Deyab, A. Vinu, Quick high-temperature hydrothermal synthesis of mesoporous materials with 3D cubic structure for the adsorption of lysozyme, Sci. Technol. Adv. Mater. 16 (2015), 024806, https://doi.org/10.1088/1468-6996/16/2/024806.

[110] D.D.E. Koyuncu, The effect of hydrothermal aging time and temperature on the structural properties of KIT-6 material, Sak. Univ. J. Sci. 25 (2021) 240–251, https://doi.org/10.16984/saufenbilder.755286.

[111] C. Santasnachok, W. Kurniawan, H. Hinode, Characterization of Thailand rice husk ash from biomass power plant and synthesized zeolite, J. Life Sci. 10 (2015), https://doi.org/10.17265/1934-7391/2015.03.006.

[112] A. Ijaz, M.B. Yagci, C.W. Ow-Yang, A.L. Demirel, A. Mikó, Formation of mesoporous silica particles with hierarchical morphology, Microporous Mesoporous Mater. 303 (2020), 110240, https://doi.org/10.1016/j.micromeso.2020.110240.

[113] M. Hasanah, T. Sembiring, K. Sebayang, S. Humaidi, T.J. Rahmadsyah, F. Saktisahdan, S.I. Handoko, Ritonga, Extraction of silica dioxide (SiO 2) from mount sinabung volcanic ash with coprecipitation method, IOP Conf. Ser.: Mater. Sci. Eng. 1156 (2021), 012015, https://doi.org/10.1088/1757-899x/1156/1/012015.

[114] N.S. Indrasti, A. Ismayana, A. Maddu, S.S. Utomo, Synthesis of nano-silica from boiler ash in the sugar cane industry using the precipitation method, Int. J. Technol. 11 (2020) 422–435, https://doi.org/10.14716/ijtech.v11i2.1741.

[115] N.N. Ngoc, L.X. Thanh, L.T. Vinh, B.T.Van Anh, High-purity amorphous silica from rice husk: preparation and characterization, Vietnam J. Chem. 56 (2018) 730–736, https://doi.org/10.1002/vjch.201800079.

[116] L. Silvia, M. Zainuri, Analisis Silika (SiO2) Hasil Kopresipitasi Berbasis Bahan Alam menggunakan Uji XRF dan XRD, JFA 16 (2020) 12, https://doi.org/10.12962/j24604682.v16i1.5322.

[117] U. Nurbaiti, S. Pratapa, Synthesis of cristobalite from silica sands of Tuban and Tanah Laut, J. Phys. Conf. Ser. 983 (2018), 012014, https://doi.org/10.1088/1742-6596/983/1/012014.

[118] M. Catauro, S. Ciprioti, Characterization of hybrid materials prepared by sol-gel method for biomedical implementations. a critical review, Materials 14 (2021) 1788.

[119] A.B.D. Nandiyanto, et al., Paper review: synthesis of nanosilica materials from various sources using various methods, J. Appl. Sci. Environ. Stud. 3 (2020) 254–278.

[120] C.A. Milea, C. Bogatu, A. Duta, The influence of parameters in silica sol-gel process, Eng. Sci. 4 (2011) 59–66.

[121] J.G. Croissant, K.S. Butler, J.I. Zink, C.J. Brinker, Synthetic amorphous silica nanoparticles: toxicity, biomedical and environmental implications, Nat. Rev. Mater. 5 (2020) 886–909, https://doi.org/10.1038/s41578-020-0230-0.

[122] G. Liang, Y. Li, C. Yang, C. Zi, Y. Zhang, X. Hu, W. Zhao, Production of biosilica nanoparticles from biomass power plant fly ash, Waste Manag 105 (2020) 8–17, https://doi.org/10.1016/j.wasman.2020.01.033.

[123] T.-H. Liou, C.-C. Yang, Synthesis and surface characteristics of nanosilica produced from alkali-extracted rice husk ash, Mater. Sci. Eng. B. 176 (2011) 521–529, https://doi.org/10.1016/j.mseb.2011.01.007.

[124] F. Adam, C. Thiam-Seng, J. Andas, A simple template-free sol–gel synthesis of spherical nanosilica from agricultural biomass, J. Sol. Gel Sci. Technol. 59 (2011) 580–583, https://doi.org/10.1007/s10971-011-2531-7.

[125] J. Davarpanah, M.H. Sayahi, M. Ghahremani, S. Karkhoei, Synthesis and characterization of nano acid catalyst derived from rice husk silica and its application for the synthesis of 3,4-dihydropyrimidinones/thiones compounds, J. Mol. Struct. 1181 (2019) 546–555, https://doi.org/10.1016/j.molstruc.2018.12.113.

[126] D. Dhaneswara, J. Fatriansyah, F. Situmorang, A. Haqoh, Synthesis of amorphous silica from rice husk ash: comparing HCl and CH3COOH acidification methods and various alkaline concentrations, IJTech 11 (2020) 200, https://doi.org/10.14716/ijtech.v11i1.3335.

[127] P. Terzioğlu, S. Yücel, B. Karakuzu İkizler, T. Temel, Y. Elalmış, Effect of Acid Type and Gelation pH on The Structural Properties of Silica Aerogels Prepared by Use of Rice Hull Biosilica, (2016).
[128] N.A. Rahman, W. Widiyastuti, D. Sigit, M. Ajiza, W. Sujana, The effect of various acids to the gelation process to the silica gel characteristic using organic silica, IOP Conf. Ser. Mater. Sci. Eng. 299 (2018), 012049, https://doi.org/10.1088/1757-899x/299/1/012049.
[129] M.E. Aphane, F.J. Doucet, R.A. Kruger, L. Petrik, E.M. van der Merwe, Preparation of sodium silicate solutions and silica nanoparticles from South African coal fly ash, Waste Biomass Valoriz. 11 (2020) 4403–4417, https://doi.org/10.1007/s12649-019-00726-6.
[130] C.K. Manchanda, R. Khaiwal, S. Mor, Application of sol–gel technique for preparation of nanosilica from coal powered thermal power plant fly ash, J. Sol. Gel Sci. Technol. 83 (2017) 574–581, https://doi.org/10.1007/s10971-017-4440-x.
[131] N. Yuan, H. Cai, T. Liu, Q. Huang, X. Zhang, Adsorptive removal of methylene blue from aqueous solution using coal fly ash-derived mesoporous silica material, Adsorpt. Sci. Technol. 37 (2019) 333–348, https://doi.org/10.1177/0263617419827438.
[132] N.K. Mermer, S. Piskin, Silica based aerogel synthesis from fly ash and bottom ash: the effect of synthesis parameters on the structure, Main. Gr. Chem. 17 (2018) 63–77, https://doi.org/10.3233/MGC-180254.
[133] F.F. De Oliveira, K.O. Moura, L.S. Costa, C.B. Vidal, A.R. Loiola, R.F. Do Nascimento, Reactive adsorption of parabens on synthesized micro- and mesoporous silica from coal fly ash: PH effect on the modification process, ACS Omega 5 (2020) 3346–3357, https://doi.org/10.1021/acsomega.9b03537.
[134] L. Simatupang, R. Siburian, P. Sitanggang, M. Doloksaribu, M. Situmorang, H. Marpaung, Synthesis and application of silica gel base on mount Sinabung's fly ash for Cd(II) removal with fixed bed column, Rasayan J. Chem. 11 (2018) 819–827, https://doi.org/10.7324/RJC.2018.1122091.
[135] N.D. Mao, S.Y. Lee, H.J. Shin, L.K. Kwac, S.C. Ko, H.G. Kim, H. Jeong, Biomass fly ash as an alternative approach for synthesis of amorphous silica nanoparticles with high surface area, J. Nanosci. Nanotechnol. 18 (2017) 3329–3334, https://doi.org/10.1166/jnn.2018.14548.
[136] L. Anggria, H.T. Masunaga, A method for production of pure silica as fertilizer from industrial waste material, IOP Conf. Ser. Earth Environ. Sci. 648 (2021), 012213, https://doi.org/10.1088/1755-1315/648/1/012213.
[137] N.P. Bhengu, Understanding Effect of Process Variables on Extraction of Silica (SiO2) from Coal Fly Ash (CFA) and Pulp Waste Ash, University of the Witwatersrand, Johannesburg, 2020.
[138] M. Sholeh, R. Rochmadi, H. Sulistyo, B. Budhijanto, Synthesis of precipitated silica from bagasse ash as reinforcing filler in rubber, IOP Conf. Ser. Mater. Sci. Eng. 778 (2020), 012012, https://doi.org/10.1088/1757-899X/778/1/012012.
[139] S. Chunsawang, Production of Silica from Biomass Ashes, in: 8th Int. Thai Inst. Chem. Eng. Appl. Chem. Conf. 2018, 2018.
[140] N. Sapawe, Production of silica from agricultural waste, Arch. Org. Inorg. Chem. Sci. 3 (2018) 342–343, https://doi.org/10.32474/aoics.2018.03.000160.
[141] D.S. Megawati, R.D. Fardhyanti, O. Artanti Putri, A.F. Fianti, A.E. Simalango Akhir, Synthesis of silica powder from sugar cane bagasse ash and its application as adsorbent in adsorptive-distillation of ethanol-water solution, MATEC Web Conf. 237 (2018) 1–6, https://doi.org/10.1051/matecconf/201823702002.
[142] V. Davina, P.S. Utama, E. Saputra, S. Bahri, Zeolite Na-P1 derived from palm oil mill fly ash: synthesis and characterization, J. Phys. Conf. Ser. 1351 (2019), 012103, https://doi.org/10.1088/1742-6596/1351/1/012103.
[143] F.Z. Haque, R. Nandanwar, P. Singh, K. Dharavath, F.F. Syed, Effect of different acids and solvents on optical properties of SiO2 nanoparticles prepared by the sol-gel process, Silicon 10 (2018) 413–419, https://doi.org/10.1007/s12633-016-9464-2.
[144] A.R.K. Gollakota, V. Volli, C.M. Shu, Progressive utilisation prospects of coal fly ash: a review, Sci. Total Environ. 672 (2019) 951–989, https://doi.org/10.1016/j.scitotenv.2019.03.337.
[145] P. Terzioğlu, S. Yücel, Ç. Kuş, Review on a novel biosilica source for production of advanced silica-based materials: wheat husk, Asia-Pacific, J. Chem. Eng. 14 (2019) 1–14, https://doi.org/10.1002/apj.2262.
[146] J.A.S. Costa, C.M. Paranhos, Mitigation of silica-rich wastes: An alternative to the synthesis eco-friendly silica-based mesoporous materials, Microporous Mesoporous Mater. 309 (2020), 110570, https://doi.org/10.1016/j.micromeso.2020.110570.
[147] F. das, C.M. da Silva, M.J. do, S. Costa, L.K.R. da Silva, A.M. Batista, G.E. da Luz, Functionalization methods of SBA-15 mesoporous molecular sieve: a brief overview, SN Appl. Sci. 1 (2019) 1–11, https://doi.org/10.1007/s42452-019-0677-z.
[148] R. Thahir, A.W. Wahab, N. La Nafie, I. Raya, Synthesis of high surface area mesoporous silica SBA-15 by adjusting hydrothermal treatment time and the amount of polyvinyl alcohol, Open Chem. 17 (2019) 963–971, https://doi.org/10.1515/chem-2019-0106.
[149] L.T. Gibson, Mesosilica materials and organic pollutant adsorption: part A removal from air, Chem. Soc. Rev. 43 (2014) 5163–5172, https://doi.org/10.1039/c3cs60096c.
[150] M.E. Adrover, M. Pedernera, M. Bonne, B. Lebeau, V. Bucalá, L. Gallo, Synthesis and characterization of mesoporous SBA-15 and SBA-16 as carriers to improve albendazole dissolution rate, Saudi Pharm. J. 28 (2020) 15–24, https://doi.org/10.1016/j.jsps.2019.11.002.
[151] A. Woszuk, R. Panek, J. Madej, A. Zofka, W. Franus, Mesoporous silica material MCM-41: Novel additive for warm mix asphalts, Constr. Build. Mater. 183 (2018) 270–274, https://doi.org/10.1016/j.conbuildmat.2018.06.177.
[152] H. Geng, Z. Mou, Z. Liu, F. Li, C. Yang, Biochemical degradation of chitosan over immobilized cellulase and supported fenton catalysts, Catalysts 10 (2020) 1–14, https://doi.org/10.3390/catal10060604.
[153] I. Díaz, J. Pérez-Pariente, O. Terasaki, Structural study by transmission and scanning electron microscopy of the time-dependent structural change in M41S mesoporous silica (MCM-41 to MCM-48, and MCM-50), J. Mater. Chem. 14 (2004) 48–53, https://doi.org/10.1039/b310281e.
[154] J. Sarkar, D. Mridha, J. Sarkar, J.T. Orasugh, B. Gangopadhyay, D. Chattopadhyay, T. Roychowdhury, K. Acharya, Synthesis of nanosilica from agricultural wastes and its multifaceted applications: a review, Biocatal. Agric. Biotechnol. 37 (2021), 102175, https://doi.org/10.1016/j.bcab.2021.102175.
[155] W. Donphai, N. Musikanon, Z. Du, P. Sangteantong, K. Chainarong, M. Chareonpanich, Preparation of C-Zn functionalized MCM-41 from bagasse heavy ash for adsorption of volatile organic compounds, Mater. Lett. 307 (2022), 131065, https://doi.org/10.1016/j.matlet.2021.131065.
[156] G. Chandrasekar, K.-S. You, J.-W. Ahn, W.-S. Ahn, Synthesis of hexagonal and cubic mesoporous silica using power plant bottom ash, Microporous Mesoporous Mater. 111 (2008) 455–462, https://doi.org/10.1016/j.micromeso.2007.08.019.
[157] J.-E. Park, H.-K. Youn, S.-T. Yang, W.-S. Ahn, CO_2 capture and MWCNTs synthesis using mesoporous silica and zeolite 13X collectively prepared from bottom ash, Catal. Today 190 (2012) 15–22, https://doi.org/10.1016/j.cattod.2011.09.032.
[158] G. Falk, G.P. Shinhe, L.B. Teixeira, E.G. Moraes, A.P.N. de Oliveira, Synthesis of silica nanoparticles from sugarcane bagasse ash and nano-silicon via magnesiothermic reactions, Ceram. Int. 45 (2019) 21618–21624, https://doi.org/10.1016/j.ceramint.2019.07.157.
[159] I.H. Nurwahid, L.C.C. Dimonti, A.A. Dwiatmoko, J.-M. Ha, R.T. Yunarti, Investigation on SiO2 derived from sugarcane bagasse ash and pumice stone as a catalyst support for silver metal in the 4-nitrophenol reduction reaction, Inorg. Chem. Commun. (2021), 109098, https://doi.org/10.1016/j.inoche.2021.109098.
[160] S.S. Hossain, P.K. Roy, Waste rice husk ash derived sol: a potential binder in high alumina refractory castables as a replacement of hydraulic binder, J. Alloy. Compd. 817 (2020), 152806, https://doi.org/10.1016/j.jallcom.2019.152806.
[161] P. Dileep, S.K. Narayanankutty, A novel method for preparation of nanosilica from bamboo leaves and its green modification as a multi-functional additive in styrene butadiene rubber, Mater. Today Commun. 24 (2020), 100957, https://doi.org/10.1016/j.mtcomm.2020.100957.
[162] C. Zhou, C. Yan, J. Zhao, H. Wang, Q. Zhou, W. Luo, Rapid synthesis of morphology-controlled mesoporous silica nanoparticles from silica fume, J. Taiwan Inst. Chem. Eng. 62 (2016) 307–312, https://doi.org/10.1016/j.jtice.2016.01.031.
[163] M. Sari Yilmaz, S. Piskin, Evaluation of novel synthesis of ordered SBA-15 mesoporous silica from gold mine tailings slurry by experimental design, J. Taiwan Inst. Chem. Eng. 46 (2015) 176–182, https://doi.org/10.1016/j.jtice.2014.09.011.
[164] B.S. Kauldhar, S.K. Yadav, Turning waste to wealth: a direct process for recovery of nano-silica and lignin from paddy straw agro-waste, J. Clean. Prod. 194 (2018) 158–166, https://doi.org/10.1016/j.jclepro.2018.05.136.
[165] X. Huang, R. Li, F. Mo, R. Zhang, W. Deng, An innovative approach to recycle boron waste by mesoporous silica production and its application in methylene blue removal, J. Environ. Chem. Eng. 9 (2021), 105327, https://doi.org/10.1016/j.jece.2021.105327.
[166] E.N. Silva, M. Cantillo-Castrillon, T.M. Dantas, Y.M. Mesquita, D.A.S. Maia, M. Bastos-Neto, W.M. Barcellos, D.C.S. Azevedo, Siloxane adsorption by porous silica synthesized from residual sand of wastewater treatment, J. Environ. Chem. Eng. 9 (2021), 104805, https://doi.org/10.1016/j.jece.2020.104805.
[167] F.C. Pa, A. Chik, M.F. Bari, Palm ash as an alternative source for silica production, MATEC Web Conf. 78 (2016), 01062.
[168] P. Deshmukh, D. Peshwe, S. Pathak, FTIR and TGA analysis in relation with the % crystallinity of the SiO_2 obtained by burning rice husk at various temperatures, Adv. Mater. Res. 585 (2012) 77–81, https://doi.org/10.4028/www.scientific.net/AMR.585.77.
[169] H. El Rassy, A.C. Pierre, NMR and IR spectroscopy of silica aerogels with different hydrophobic characteristics, J. Non Cryst. Solids 351 (2005) 1603–1610, https://doi.org/10.1016/j.jnoncrysol.2005.03.048.
[170] M.N.A. Uda, S.C.B. Gopinath, U. Hashim, N.H. Halim, N.A. Parmin, M.N. Afnan Uda, P. Anbu, Production and characterization of silica nanoparticles from fly ash: conversion of agro-waste into resource, Prep. Biochem. Biotechnol. 51 (2021) 86–95, https://doi.org/10.1080/10826068.2020.1793174.
[171] C. Galacho, M.M.L. Ribeiro Carrott, P.J.M. Carrott, Evaluation of the thermal and mechanical stability of Si-MCM-41 and Ti-MCM-41 synthesised at room temperature, Microporous Mesoporous Mater. 108 (2008) 283–293, https://doi.org/10.1016/j.micromeso.2007.04.010.
[172] X. Castillo, J. Pizarro, C. Ortiz, H. Cid, M. Flores, E. De Canck, P. Van Der Voort, A cheap mesoporous silica from fly ash as an outstanding adsorbent for sulfate in water, Microporous Mesoporous Mater. 272 (2018) 184–192, https://doi.org/10.1016/j.micromeso.2018.06.014.
[173] P. Sikarwar, U.K.A. Kumar, V. Gosu, V. Subbaramaiah, Catalytic oxidative desulfurization of DBT using green catalyst (Mo/MCM-41) derived from coal fly ash, J. Environ. Chem. Eng. 6 (2018) 1736–1744, https://doi.org/10.1016/j.jece.2018.02.021.
[174] S. Porrang, N. Rahemi, S. Davaran, M. Mahdavi, B. Hassanzadeh, A.M. Gholipour, Direct surface modification of mesoporous silica nanoparticles by DBD plasma as a green approach to prepare dual-responsive drug delivery system, J. Taiwan Inst. Chem. Eng. 123 (2021) 47–58, https://doi.org/10.1016/j.jtice.2021.05.024.

[175] N. Waheed, A. Mushtaq, S. Tabassum, M.A. Gilani, A. Ilyas, F. Ashraf, Y. Jamal, M.R. Bilad, A.U. Khan, A.L. Khan, Mixed matrix membranes based on polysulfone and rice husk extracted silica for CO_2 separation, Sep. Purif. Technol. 170 (2016) 122–129, https://doi.org/10.1016/j.seppur.2016.06.035.

[176] B. Wang, Y. Zhou, L. Li, Y. Wang, Preparation of amidoxime-functionalized mesoporous silica nanospheres (ami-MSN) from coal fly ash for the removal of U (VI), Sci. Total Environ. 626 (2018) 219–227, https://doi.org/10.1016/j.scitotenv.2018.01.057.

[177] S.K. Hubadillah, M.H.D. Othman, A.F. Ismail, M.A. Rahman, J. Jaafar, Y. Iwamoto, S. Honda, M.I.H.M. Dzahir, M.Z.M. Yusop, Fabrication of low cost, green silica based ceramic hollow fibre membrane prepared from waste rice husk for water filtration application, Ceram. Int. 44 (2018) 10498–10509, https://doi.org/10.1016/j.ceramint.2018.03.067.

[178] W. Henao, L.Y. Jaramillo, D. López, M. Romero-Sáez, R. Buitrago-Sierra, Insights into the CO2capture over amine-functionalized mesoporous silica adsorbents derived from rice husk ash, J. Environ. Chem. Eng. 8 (2020), 104362, https://doi.org/10.1016/j.jece.2020.104362.

[179] R. Jothi Ramalingam, J.N. Appaturi, T. Pulingam, H.A. Al-Lohedan, D.M. Al-dhayan, In-situ incorporation of ruthenium/copper nanoparticles in mesoporous silica derived from rice husk ash for catalytic acetylation of glycerol, Renew. Energy 160 (2020) 564–574, https://doi.org/10.1016/j.renene.2020.06.095.